HHS Public Access

Author manuscript

Dev Dyn. Author manuscript; available in PMC 2024 January 01.

Published in final edited form as:

Dev Dyn. 2023 January ; 252(1): 124–144. doi:10.1002/dvdy.548.

Cochlear hair cell innervation is dependent on a modulatory function of Semaphorin-3A

Homero L. Cantu-Guerra[1,2], **Michael R. Papazian**[1], **Anna L. Gorsky**[1], **Nathalie S. Alekos**[1], **Adam Caccavano**[2,3], **Nare Karagulyan**[4], **Jakob Neef**[4], **Stefano Vicini**[2,3], **Tobias Moser**[4], **Thomas M. Coate**[1,2]

[1]Department of Biology, Georgetown University, Washington, District of Columbia, USA

[2]Interdisciplinary Program in Neuroscience, Georgetown University, Washington, District of Columbia, USA

[3]Department of Pharmacology, Georgetown University School of Medicine, Washington, District of Columbia, USA

[4]Institute for Auditory Neuroscience and InnerEarLab, University Medical Center, and Auditory Neuroscience & Synaptic Nanophysiology Group, Max Planck Institute for Multidisciplinary Sciences, and Cluster of Excellence “Multiscale Bioimaging: from Molecular Machines to Networks of Excitable Cells” (MBExC), Göttingen, Germany

Abstract

Background: Proper connectivity between type I spiral ganglion neurons (SGNs) and inner hair cells (IHCs) in the cochlea is necessary for conveying sound information to the brain in mammals. Previous studies have shown that type I SGNs are heterogeneous in form, function and synaptic location on IHCs, but factors controlling their patterns of connectivity are not well understood.

Results: During development, cochlear supporting cells and SGNs express Semaphorin-3A (SEMA3A), a known axon guidance factor. Mice homozygous for a point mutation that attenuates normal SEMA3A repulsive activity (*Sema3a*^{K108N}) show cochleae with grossly normal patterns of IHC innervation. However, genetic sparse labeling and three-dimensional reconstructions of individual SGNs show that cochleae from *Sema3a*^{K108N} mice lacked the normal synaptic distribution of type I SGNs. Additionally, *Sema3a*^{K108N} cochleae show a disrupted distribution of

Correspondence: Thomas M. Coate, Department of Biology, Georgetown University, 37th and O St. NW, Washington, DC 20007, USA. tmc91@georgetown.edu.

AUTHOR CONTRIBUTIONS

Homero Lael Cantu-Guerra: Conceptualization (equal); data curation (lead); formal analysis (lead); investigation (lead); writing – original draft (lead); writing – review and editing (lead). **Michael Papazian:** Formal analysis (supporting); investigation (supporting). **Anna Gorsky:** Formal analysis (supporting); investigation (supporting). **Nathalie S. Alekos:** Formal analysis (supporting); methodology (supporting). **Adam Caccavano:** Formal analysis (supporting); methodology (supporting). **Nare Karagulyan:** Formal analysis (lead); investigation (lead); methodology (lead); writing – original draft (lead). **Jakob Neef:** Formal analysis (supporting); investigation (supporting); methodology (supporting); project administration (supporting). **Stefano Vicini:** Project administration (supporting); supervision (supporting). **Tobias Moser:** Funding acquisition (lead); investigation (supporting); methodology (supporting); project administration (supporting); supervision (lead); writing – review and editing (supporting). **Thomas Coate:** Conceptualization (supporting); funding acquisition (lead); methodology (supporting); project administration (lead); supervision (lead); writing – original draft (supporting); writing – review and editing (supporting).

CONFLICT OF INTEREST

The authors declare no conflict of interest.

GLUA2 postsynaptic patches around the IHCs. The addition of SEMA3A-Fc to postnatal cochleae led to increases in SGN branching, similar to the effects of inhibiting glutamate receptors. Ca^{2+} imaging studies show that SEMA3A-Fc decreases SGN activity.

Conclusions: Contrary to the canonical view of SEMA3A as a guidance ligand, our results suggest SEMA3A may regulate SGN excitability in the cochlea, which may influence the morphology and synaptic arrangement of type I SGNs.

Keywords

auditory; axon guidance; cochlea; ribbon synapse; Semaphorin; spiral ganglion neuron

1 | INTRODUCTION

The mammalian cochlea provides a tractable model of the spatial patterning of neuronal circuits because it is composed of numerous cell types precisely arranged to transmit sound stimuli to the CNS.[1] In the cochlea, spiral ganglion neurons (SGNs) extend peripheral axons (also known as “dendrites”) that form ribbon-type synapses with hair cells, and central axons that extend into the dorsal and ventral cochlear nuclei. Previous studies have detailed the differentiation and morphological development of hair cells, SGNs, and the synapses that join them.[2–6] There are two major groups of SGNs in the mammalian cochlea. Type I SGNs, which constitute around 95% of the total population, are myelinated, and form synapses with only inner hair cells (IHCs).[7] Type II SGNs, the remaining 5%, are unmyelinated and form synapses with multiple outer hair cells (Figure 1C).[8,9] Previously, we and others documented how type I and II SGNs segregate their peripheral termini between E16.5 and P0.[5] We also documented how type I SGNs undergo branch refinement between E15.5 and hearing onset.[10] Single cell labeling and electrophysiological studies in the cat auditory nerve have found that type I SGNs differ in sensitivity, spontaneous rate (SR), and fiber diameter.[2] Based on these findings, they were classified into three groups: low-SR, medium-SR, and high-SR.[7] Noteworthy from these studies was how type I SGNs with different excitability characteristics tended to form synapses on different sides of the IHC: high-SR SGNs tended to make contact with the pillar cell side of the IHC, whereas low-SR SGNs tended to make contact with the modiolar side of the IHC. More recent single-cell transcriptome studies showed that type I SGNs differentiate into three populations based on distinguishable mRNA signatures.[11–13] However, the molecular mechanisms underlying the spatial patterning of SGNs during their maturation and innervation of hair cells remain to be elucidated.

Semaphorins are axon-guidance ligands that play various roles in the developing nervous system and interact with Neuropilin (NRP) and Plexin (PLXN) receptors. Previously, we reported on the developmental role of SEMA3F,[5] which acts through NRP2 to limit the number of SGN projections that innervate outer hair cells. In addition, we have found that SEMA5B is expressed by hair cells to control SGN branch refinement.[10] As described in this report, we have found that Semaphorin-3A (SEMA3A) plays a role distinct from either SEMA3F or −5B. SEMA3A was one of the first secreted repulsive guidance factors to be characterized[14] and plays a crucial role in the regulation of growth cone motility, dendrite development, maturation, and signals mainly through NRP1.[15,16] NRP1 is a transmembrane

receptor known to interact with both vascular endothelial growth factors (VEGFs) and various subtypes of Semaphorins including 3A, 3B, 3C, and 3D.[16–19] During early stages of inner ear development, *Nrp1* mutants show dramatic cochlear innervation patterning defects and a progressive loss of SGNs, suggesting NRP1 plays a role in SGN axon guidance and survival.[20] But, it is not clear what aspects are mediated by the different SEMAs that bind NRP1.

SEMA3A has been found to serve numerous roles in the nervous system besides chemorepulsion: it refines odor maps in the olfactory bulb, promotes maturation of dendritic spines in the cerebral cortex, and regulates AMPA receptor expression in the hippocampus.[21–23] In the inner ear, SEMA3A may similarly employ a differential mechanism of regulation, as it has been shown to alter SGN membrane excitability in vitro.[24] In this study, we show that SEMA3A is necessary for the development of type I SGNs and their synaptic connections with IHCs. Here, we show that *Sema3a* is expressed by cochlear supporting cells and SGNs during embryonic and early postnatal development. We examined a *Sema3a* mutant mouse model ("*Sema3a*^{K108N}") where a SEMA3A point mutant binds to NRP1 but cannot activate downstream signaling mechanisms.[25] Notably, the *Sema3a*^{K108N} mutants phenocopy *Sema3a* null mutants without appearing to have any additional phenotypes.[25] Our results suggest that SEMA3A normally promotes the development of type I SGNs by influencing their morphology and synaptic arrangement of type I SGNs, possibly through activity modulation.

2 | RESULTS

2.1 | Developmental changes in type I SGN fiber diameter on the modiolar and pillar cell sides of the IHC

The organ of Corti is composed of a single row of IHCs and three rows of OHCs, which are innervated by type I and type II SGNs, respectively. SGNs are morphologically bipolar neurons, which extend their peripheral axons to the hair cells and central axons toward the cochlear nucleus in the CNS. Figure 1A show a whole mount view of the cochlear sensory domain, where SGNs are labeled with Tuj1 antibodies, and the hair cells labeled with anti-Myosin VI antibodies. In the immature cochlea, type I SGNs form numerous exploratory branches around the inner and outer hair cells.[5] These branches go through an extensive refinement before hearing onset (~P10–12 in mouse) leading to a single bouton ending with an IHC. In the mature mouse cochlea, a single IHC shows contact with around 20 type I SGNs.[26] The transient immature branches of type I SGNs can be appreciated on SGNs that have been labeled sparsely using *Bhlhb5*^{Cre} and *Rosa26*^{MORF3} (Figure 1B). Previously, it was shown that type I SGNs with larger diameter fibers tend to form synapses on the pillar cell side of the IHC, whereas thinner type I SGN fibers tend to form synapses on the side of the IHC closer to the modiolus (Figure 1C).[6] To determine when this spatial segregation of type I SGNs (based on fiber diameter) was apparent, we examined sparsely labeled type I SGNs at E17.5, P0, P2, P4, P6, P8, P15, P19, and P28. In this series, *Neurog1*^{CreERT2} and *R26R*^{tdTomato} were used as we have done previously (Jung et al., 2019; see also Figure 4). Samples were also stained with either anti-Myosin-VI or -VIIa antibodies for hair cell identification. Imaris software was used to track fibers to the "modiolar" or "pillar cell" side

of the IHC and determine their diameter. As shown in Figure 1D, the maturation of type I SGN morphology is dynamic, and goes through a period of size fluctuations through P28. We note here that the fiber diameter measurements for each stage were normalized to the average values of the fibers on the modiolar side of the IHCs. This allowed us to compare trends between stages. Since the analysis using Imaris uses fluorescence intensity to measure size, and since there is variability in sample thickness at different stages, we felt it would be inappropriate to compare absolute values. At E17.5, both thin and thick fibers are visible, but are not positioned around the IHC based on size. However, at P0 and P2, the SGNs synapsing on the pillar cell side of the IHC are overall thicker than those on the modiolar side, but both populations show overlapping fiber diameters. Interestingly, the relative fiber diameter of each population appears to reverse from P8 through P19. They then reestablish a mature pattern around P28. So, despite the cochlea being fully functional around P12, the morphology of type I SGNs appears to fluctuate. In correspondence with these findings, presynaptic ribbon puncta and postsynaptic glutamate receptor spots were shown to fluctuate by volume based on IHC side around the same time periods.[27]

2.2 | SEMA3A and NRP1 show a complementary distribution around the cochlear sensory domain during development

Transcriptome studies (unpublished) of genes expressed in the cochlea during development showed that *Sema3a* was upregulated during periods of hair cell innervation. This data led us to examine the distribution of *Sema3a* by in situ hybridization and immunohistochemistry in cross sections of cochleae from different time points (Figure 2). At E12.5, before development of hair cells, *Sema3a* was found to be highly expressed by SGNs and broadly distributed in the cochlear epithelium (Figure 2A). However, at E14.5 and E16.5, when the SGNs begin to make contact with early hair cells, S*ema3a* continues to be expressed by SGNs, but becomes more narrowly expressed in the sensory epithelium, specifically in inner phalangeal cells and lesser epithelial ridge cells (Figure 2B–D). At P4, *Sema3a* expression persists in both sensory epithelia and SGNs, but appears reduced compared to earlier stages (Figure 2E,F). To further determine the distribution of *Sema3a*, we immunostained the samples at E16.5 using anti-MyoVI antibodies to identify hair cells. To localize SEMA3A protein, we then immunostained E17.5 (not shown) and P4 cochlear cross sections with anti-SEMA3A antibodies. At both stages, SEMA3A protein was distributed outside of the base of the IHCs in a filament-like manner, which overlapped with neurofilament-positive SGN peripheral terminals (Figure 2I–K). SEMA3A also seemed to be prominent around the SGN cell bodies (Figure 2L), similar to the position of *Sema3a* mRNA in the SGN cytosol. These data suggest SEMA3A may be involved in the development of connectivity between SGNs and hair cells.

Previous work in dorsal root ganglion cells and other systems, has shown that NRP1 can function as a receptor for SEMA3A.[16] In the cochlea, in situ hybridization data showed expression of *Nrp1* during pre and post-natal stages.[20] To determine if NRP1 protein expression overlaps spatially and temporally with SEMA3A, we immunostained developing cochleae with anti-NRP1 antibodies. At E16.5, NRP1 protein was present on SGNs, as indicated by overlap with Tuj1 staining (Figure 3A–C). In addition, NRP1 protein was present at high levels on blood vessels of the cochlea, which is expected because as it plays

roles in vascular development in many systems.[15] To examine whether SEMA3A binds to type I SGNs, we performed a "ligand-binding assay" where recombinant SEMA3A-Fc was applied to lightly fixed E17.5 cochlear tissue then detected with anti-Fc antibodies. As shown on Figure 3D–F, the anti-Fc staining is only visible on SGN fibers (D) and cell bodies (F), but not blood vessels. We next stained P0 cochlear cross sections with anti-NF200, -SEMA3A, and -NRP1 antibodies to determine if SEMA3A and NRP1 are distributed similarly on SGN fibers. Indeed, all three factors showed overlap around the base of the IHCs, where synapses are distributed (Figure 3G–J). These data suggest that SEMA3A may act on SGNs during development, possibly by interacting with NRP1.

2.3 | *Sema3a*^{K108N} mice show type I SGN morphology changes around IHCs

To begin to investigate SEMA3A function in vivo, we first examined cochleae from the *Sema3a*^{K108N} mouse line. Mice carrying this point mutation mimic *Sema3a* knockout mice in the sense that the interactions between the K108N variant of SEMA3A and NRP1 does not lead to any downstream cellular effects.[25] Previous work on *Sema3a* null mice showed defects in afferent projections within the vestibular ganglia.[28] but defects in SGNs were not reported. We first evaluated the *Sema3a*^{K108N} cochleae for general cochlear innervation phenotypes. Compared with littermate controls at P2, *Sema3a*^{K108N} cochleae showed an overall normal morphology and distribution of SGNs and hair cells (Figure 4A–D; Tuj1 and MyoVI staining). We also measured the length of Rosenthal's canal and found no differences suggesting the *Sema3a*^{K108N} cochleae extend normally (Figure 4E). Previously, we found that SGN afferents and olivocochlear efferents could be distinguished by anti-SYT1 and anti-GAP43, respectively.[5] Compared to controls, the *Sema3a*^{K108N} cochleae showed no dramatic innervation defects by either afferent or efferent fibers (Figure 4F–I). When we quantified the number of type II SGNs crossing into the OHC region, we found a small but statistically significant reduction in the base of the mutants, but not in other turns (Figure 4F,H,J). Overall, this difference was very minor. Single-cell RNA sequencing analyses have identified three major subpopulations of type I SGNs.[11–13] To determine if the *Sema3a*^{K108N} cochleae showed any change in the proportion of these subtypes, we immunostained P30 cochlear cross sections with antibodies that target Calretinin (Calb2; type Ia), Calbindin (Calb1; type 1b), and Ly6/PlAUR domain-containing protein 1 (LYPD1; type Ic). Compared to controls, *Sema3a*^{K108N} cochleae showed no significant shifts in overall subtype populations (Figure 4K,L), suggesting SEMA3A signaling is dispensable for SGN subtype differentiation.

To further investigate the potential contribution of SEMA3A signaling on type I SGNs during development, the *Sema3a*^{K108N} mouse line was crossed to mice carrying *Neurog1*^{CreERT2} and *Rosa26*^{tdTomato} for detailed morphological analyses of single neurons (Figure 4M). In the WT cochleae at P2, at both the base and apex, the fiber diameter of type I SGNs synapsing at the modiolar side of the IHCs were thinner than those synapsing at the pillar cell side (Figure 4N; left panel). We decided to use P2 since it was the earliest instance there was a noticeable diameter change between modiolar and pillar SGN fibers (Figure 1). Notably, the *Sema3a*^{K108N} type I SGNs lacked the typical "bimodal" distribution (Figure 4N; right panel): at the cochlear apex and base in this mutant, we found no statistically significant differences in fiber diameter between neurons synapsing on either side of the hair

cell. These data suggest that SEMA3A is needed for the normal spatial distribution of type I SGNs with peripheral axons of different diameters.

2.4 | *Sema3a*^{K108N} mice show comparatively larger GLUA2 patches on the modiolar side of the IHC

We next asked whether the changes of type I SGN morphology seen at P2 might accompany postsynapse morphology changes in later stages. To address this, we used anti-CTBP2 antibodies to identify the IHC synaptic region, and anti-GLUA2 antibodies to identify postsynaptic patches on type I SGNs of *Sema3a*^{K108N} mice and littermate controls. Previous studies demonstrated size gradients of postsynaptic GLUA2 patches based on their position (pillar vs modiolar) around the IHC, and that the spatial distribution of these gradients changed over the course of development, becoming stable by P30.[27] Using Imaris software, we individually reconstructed GLUA2 puncta from *Sema3a*^{K108N} cochleae and their littermate controls at P28-P30 (Figure 5A–F), mapping them to pillar and modiolar sides of the IHC (Figure 5H) and then compared their sizes (μm^3). For this analysis, we avoided synapses that were positioned at the very habenular pole of the IHC because it was difficult to classify them as “pillar” or “modiolar.” In addition, we only included in this analysis postsynapse patches that were spatially isolated and adjacent to individual CtBP2 ribbon bodies. Control cochleae tend to show larger (but not with statistical significance) GLUA2 patches on the pillar cell side of the IHC (Figure 5I). However, in *Sema3a*^{K108N} cochleae this pattern was reversed: higher volume GLUA2 patches were found closer to the modiolar side of the IHCs (Figure 5I) and were larger (with statistical significance) compared to the same population in controls. These results support a model whereby SEMA3A in the cochlea regulates the maturation of type I SGNs and is needed for normal patterns of GLUA2 distribution.

2.5 | Average properties and heterogeneity of Ca^{2+} influx at IHC active zones are mostly unaffected in *Sema3a*^{K108N} cochleae

Previously, loss of *Pou4f1* in SGNs led to altered Ca^{2+} influx properties at IHC active zone (AZ), which indicated a possible instructive role for SGNs on developing hair cells.[29] Given this and our observations that SGNs were affected in the *Sema3a*^{K108N} cochleae, we next examined whether the *Sema3a*^{K108N} mice showed altered IHC Ca^{2+} influx properties. We first examined whole-cell evoked Ca^{2+} currents in IHCs from 4-week-old mice by applying voltage step depolarizations from −82 to 63 Mv (Figure 6A). Maximal Ca^{2+} influx amplitudes tended to be increased in *Sema3a*^{K108N} IHCs compared to littermate controls without reaching statistical significance. Additionally, we analyzed the voltage dependence of Ca^{2+} channel activation in *Sema3a*^{K108N} IHCs and found no significant difference compared to controls (Figure 6B). We next measured Ca^{2+} influx at single presynaptic AZs as we have done previously.[30] IHCs were first loaded with both Fluo-4FF (a low affinity Ca^{2+}-indicator) and TAMRA-conjugated Ctbp2 binding peptide for the identification of presynaptic AZs (Figure 6C).[26,29,31] We then visualized Ca^{2+} influx evoked by voltage ramp depolarizations to assess amplitude and voltage dependence of Ca^{2+} influx at individual IHC AZs. While the AZs from *Sema3a*^{K108N} IHCs were on average similar to controls in terms of the Ca^{2+} influx amplitude and voltage of half maximal activation (Figure 6D), they showed a slight but significant increase in voltage sensitivity (Figure 6E). We consider it

unlikely that this slight change results in a significant biological difference in IHC glutamate release properties. We next reconstructed the IHCs in cylindrical coordinate system that identified modiolar vs pillar synaptic position.[30] Synapses located on the modiolar side of IHCs normally show elevated maximum Ca^{2+} influx and depolarized activation of Ca^{2+} channels compared to the synapses on the pillar side of the IHCs.[26,30] In these experiments, this gradient was present in both controls and *Sema3a*^{K108N} IHCs to a similar degree (Figure 6F,G). These data suggest that *Sema3a*^{K108N} cochleae show normal hair cell Ca^{2+} influx properties both on whole cell and single AZ level. Moreover, the position-dependent differences of AZs in Ca^{2+} influx seem to be maintained despite the apparent developmental changes in SGNs.

As part of these experiments, we also analyzed the modiolar vs pillar distribution of CtBP2 binding peptide fluorescence of AZs in each of the IHCs for that which synaptic Ca^{2+} influx was assessed. As shown previously,[30] presynaptic spots that are labeled with the CtBP2 binding peptide showed greater fluorescence intensity when located on the modiolar side of the IHC. This was interpreted as indicating larger ribbons on the modiolar side as (a) it was also found for anti-CtBP2 immunofluorescence intensity and (b) the anti-CtBP2 immunofluorescence intensity increase over IHC developmental in parallel to an enlargement of ribbons as measured with transmission electron microscopy.[32] As expected, WT IHCs showed increased Ctbp2 binding peptide fluorescence intensity values on the modiolar side of the IHC. Interestingly, the fluorescence intensity gradient of the CtBP2 binding peptide in the *Sema3a*^{K108N} IHCs was comparable to that of WT IHCs (Figure 7A,B). This corroborates the finding that Ca^{2+} influx properties between WT and *Sema3a*^{K108N} IHCs are unchanged, further suggesting that hair cells are unaffected in *Sema3a*^{K108N} cochleae.

2.6 | Exogenous SEMA3A increases type I SGN branch number in vitro, an effect similar to glutamate receptor inhibition

Given the changes to SGN fiber and synapse size observed in the *Sema3a*^{K108N} cochleae, we predicted SEMA3A signaling might control aspects of type I SGN morphological development. To examine this, we cultured cochleae from P4 neonates containing the *Neurog1*^{CreERT2} and *R26R*^{Tdtomato} alleles for 24 hours in the presence of either control IgG-Fc or SEMA3A-Fc (each at 20 nM). Fc-conjugated Semaphorins have been shown previously to bind their cognate receptors and induce signaling.[33] Following fixation, samples were labeled with anti-dsRed antibodies, imaged using confocal microscopy, and analyzed in Imaris for fiber diameter and branch number. SEMA3A-Fc had no effect on SGN fiber thickness (not shown), which was surprising given how SGN thickness was altered in the *Sema3a* mutants. But, it is possible that changes in fiber diameter would require a culture time longer than 24 hours. There also appeared to be no SGN collapse response, which we observed previously in embryonic cochleae following SEMA3A-Fc treatment.[20] Unexpectedly, compared to controls, SEMA3A-Fc led to increased numbers of type I SGN branches (Figure 8A,B). Recently, it was shown that treating postnatal SGNs in culture with SEMA3A-Fc reduced their excitability characteristics.[24] So, we hypothesized that the increase in SGN branching we observed after SEMA3A-Fc treatment could be an effect of reduced activity. To test this hypothesis, we performed similar experiments, but

with low concentrations of NBQX and CPP, inhibitors of AMPA and NMDA receptors respectively. Compared to DMSO controls, cochleae treated with NBQX and CPP showed significant increases in SGN branch numbers, similar to those treated with SEMA3A-Fc (Figure 8B). The similarities in SGN response to SEMA3A-Fc and NBQX/CPP treatment (increased branch numbers) suggest the possibility that Semaphorin signaling inhibits activity.

2.7 | Semaphorin-3A modifies neuronal activity in vitro

To test the hypothesis that Semaphorin signaling inhibits activity, we performed a series of experiments whereby semi-intact cultured cochleae with a fluorescent Ca^{2+} indicator (Fluo4-AM) were exposed to either soluble SEMA3A-Fc or Control-Fc. Experiments were performed using cochleae from P4 mice, which corresponds to the period in which SGNs undergo branch refinement[10] and fire spontaneously in response to glutamate released by IHCs.[34,35] Cultured cochleae were recorded first in artificial cerebrospinal fluid (ACSF) alone for 10 minutes to obtain baseline Ca^{2+} fluorescence measurements. Following the baseline recordings, each sample was exposed for 10 minutes with soluble SEMA3A-Fc or Control-Fc, then recorded for an additional 10 minutes. We used ImageJ to identify ROIs (SGN cell bodies) and then measured fluorescence changes across time. Ca^{2+} fluorescence changes were then quantified using previously published MATLAB scripts (Figure 9A,B).[36] In general, we found small-to-moderate decreases in Ca^{2+} florescence between baseline and Fc-exposed samples due to photobleaching. Compared to the Fc alone treatment group, cochleae exposed to SEMA3A-Fc showed reduced numbers of active cells, and Ca^{2+} events (active ROIs only) that were significantly smaller in amplitude and frequency, but not duration (Figure 9C). These data, showing that SGN $Ca2^{+}$ transients were diminished in the presence of SEMA3A-Fc, suggest that endogenous SEMA3A could modify SGN activity in vivo.

2.8 | *Sema3a*^{K108N} cochleae do not show altered SGN Ca^{2+} transients

To further analyze the effects of SEMA3A in the developing cochlea, we compared SGN Ca^{2+} transients from cochleae of *Sema3a*^{K108N} mice and their heterozygous littermates as controls. Similar to the experiments in Figure 9, we incubated semi-intact cultured P4 cochleae with Flou-4 AM. Cochleae from both genotypes were imaged in ACSF for 10 minutes. We then identified individual ROIs (SGN cell bodies) using ImageJ to measure fluorescence changes over time (Figure 10A,B). Although it appeared that many of the traces in the mutants were longer in duration, they were not statistically different compared to controls (Figure 10B; mean duration, $P = .07$). In addition, we did not find any significant differences between *Sema3a*^{K108N} mice and heterozygous littermate controls in the context of event mean amplitude, frequency, or number of active cells (Figure 10B). While we predict SEMA3A may have an impact on the regulation of SGN activity during development, the *Sema3a*^{K108N} mice in this experiment did not show differences that would support that hypothesis. These experiments are interpreted further in the following section.

3 | DISCUSSION

The developing nervous system requires a multitude of intra- and extracellular cues to acquire proper morphology and connectivity. The early phases of developmental wiring in the cochlea (roughly E14.5 through P0) involve events such as SGN extension toward the hair cells,[4,37] glial-guided growth and fasciculation,[38,39] and selective hair cell wiring.[5,40,41] During this period, each type I SGN exhibits an elaborate branch morphology that becomes refined into a single synaptic connection with an IHC, a process that (in part) requires SEMA5B[10] and purinergic signaling.[42] The results presented here demonstrate that SEMA3A plays a distinct and nuanced role in SGN development in that it is necessary for proper synaptic maturation of type I SGNs, and that it may do this via activity modulation.

As shown in Figure 1, the relative diameter of type I SGN fibers on the modiolar and pillar cell sides of the IHC changes between E17.5 through P28. Interestingly, the timing of these changes roughly coincides with reported fluctuations in the spatial distributions of ribbon pre- and postsynaptic puncta based on size.[27] What influences these changes prior to hearing onset is likely a complex milieu of signaling mechanisms that involves events such as SGN specification,[12,13,35] spontaneous activity, myelination,[43] and synaptic pruning.[44] In addition, the type I terminals may migrate back and forth from each side of the IHC, but difficult time-lapse studies of cochlear explants over several days would need to be performed to assess that possibility. Here, we show that the period of SEMA3A expression in the cochlea spans embryonic and early postnatal stages (Figures 2 and 3), and that loss of SEMA3A signaling led to altered patterns of IHC innervation. In particular, *Sema3a*^{K108N} cochleae did not show the normal pattern of larger-diameter type I SGN fibers on the pillar cell side of the IHC at P2 (Figure 4), nor did they show the normal spatial distribution of postsynaptic patches (based on volume) at P30 (Figure 5). These defects did not appear to confer altered IHC presynaptic Ca^{2+} activation (Figures 6 and 7), which was shown previously in the context of the loss of Pou4f1, a transcription factor expressed by a subset of type I SGNs.[29] Since Pou4f1 is a transcription factor, it may control the expression of a relatively broad set of signaling factors in SGNs, including those that may influence (in trans) aspects of hair cell development. In vitro, type I SGNs showed increased numbers of small branch protrusions after SEMA3A-Fc application, an effect that was similar to treatments with AMPA and NMDA receptor antagonists (Figure 8). As described below, SEMA3A-Fc treatments also suppressed spontaneous SGN Ca^{2+} transients (Figure 9), which supports a model whereby SEMA3A modulates activity in the developing cochlea.

3.1 | *Sema3a* is not necessary for repulsive axon guidance in the cochlea in vivo

In the nervous system, SEMA3A is most commonly known as a repulsive guidance factor that induces growth cone collapse through the NRP1 receptor.[16] In the cochlea, *Sema3a* mRNA was present as early as E12.5 (Figure 2), which corresponds to the very early stages of SGN growth and guidance.[45] Previously, we reported that *Nrp1* mutant cochleae show dramatic SGN fasciculation and hair cell targeting defects.[20] We also showed that SEMA3A-Fc caused the collapse of Tuj1-positive SGN peripheral terminals in cultured cochleae at E17.5.[20] So, it was unexpected that the *Sema3a*^{K108N} cochleae showed no gross cochlear innervation defects (Figure 4). In contrast with our previous findings using

embryonic tissue, adding soluble SEMA3A-Fc to cultured cochleae at P2 in this study did not induce SGN collapse (Figure 8). Why SGNs at E17.5 vs P2 respond differently to SEMA3A-Fc remains unclear. But, as it stands, SEMA3A does not appear to exert a significant guidance function in vivo, or it is possible that other Semaphorins compensate for the loss of normal SEMA3A signaling in the *Sema3a*^{K108N} mutants. Other secreted Semaphorins known to interact with NRP1 are also expressed in the cochlea during this time, including SEMA3C and −3D.[5] Another possibility is that NRP1 exerts SGN guidance effects following activation by VEGF, which is known to signal through NRP1 in the developing visual system.[46]

While the *Sema3a*^{K108N} mutants did not show gross cochlear innervation defects, there were clear differences in the hair cell synaptic positions of SGN fibers of different diameters (Figure 4). Prior studies show that Semaphorins can regulate different aspects of synaptic architecture. For example, visual cortex neurons in the corticospinal tract require SEMA3F and PLEXINA3 to undergo stereotyped pruning processes.[47] Additionally, *Plxna3* mutants do not exhibit typical pruning events of the hippocampal infrapyramidal neurons, and addition of exogenous SEMA3A induces increased branch retraction in CA1 neurons.[48] Previously, we found that SEMA3F is expressed in the OHC region of the cochlea and plays a role in selective hair cell innervation by repelling type I SGNs toward the IHC region.[5] Loss of SEMA3A signaling did not appear to substantially alter inner- vs outer hair cell innervation patterns (Figure 4). In addition, we previously reported that SEMA5B is expressed by hair cells and appears to function in SGN branching refinement.[10] The addition of SEMA5B-Fc to cultured cochleae reduced SGN branch numbers, while *Sema5b* knockout cochleae showed elevated SGN branch numbers. As shown in Figure 8, when SGNs were challenged with SEMA3A-Fc in vitro, they showed an increase in SGN branch number, the opposite effect of SEMA5B-Fc treatment. As noted below, this effect was similar to the effects of treating SGNs with AMPA and NMDA receptor antagonists (Figure 8). Type I SGNs from the *Sema3a*^{K108N} cochleae did not show visible branch refinement defects (not shown) nor did they show defects in selective hair cell innervation. So, our data suggest that SEMA3A functions differently than either SEMA5B or SEMA3F.

3.2 | SEMA3A may play a role in type I SGN development via activity modulation

Semaphorin-mediated changes in neural activity is not without precedent. Recently, it was shown that SEMA3F/NRP2 interactions mediate AMPA receptor homeostatic downscaling in the cortex.[49] In cultured SGNs, SEMA3A was shown previously to attenuate membrane excitability[24]: recombinant SEMA3A was applied to dissociated postnatal SGNs and generated a higher resting potential, higher firing threshold, decreased spiking amplitude, and prolonged latency and duration of spiking events. Here, we show SEMA3A-Fc treatment to SGNs reduces some aspects of spontaneous Ca^{2+} transient in postnatal cochleae (Figure 9). In particular, we found that SEMA3A-Fc reduces the numbers of actively firing SGNs overall, and reduces the amplitude and frequency of Ca^{2+} transients of remaining active neurons. Moreover, when we exposed SGNs to SEMA3A-Fc, it resulted in an increase of SGN branch numbers, similar to the effects of AMPA and NMDA channel blockers (Figure 8). The cochlear culture experiments described in Figure 8 were performed with samples starting at P4. At this stage of development, the SGNs are in the middle of a

long period of branching refinement: at E15.5, the SGN peripheral axons show numerous branches, which are slowly removed until P21. At P21, each axon is seen with only a single bouton ending making contact with one IHC.[42] While we have found that SGN branch refinement is driven by both SEMA5B[10] and P2RX3,[42] the extent to which activity is also involved is unknown. Since P4 is a period when the SGNs show spontaneous bursts of action potentials driven by glutamate,[34,35] it is possible that excitation helps drive branching refinement. These effects are similar to what has been documented in retinal ganglion cells, which show spontaneous activity prior to the presence of functional photoreceptors.[50,51] In particular, inhibiting retinal activity using tetrodotoxin leads to a retention of ectopic branches.[52] The singly labeled SGNs treated with SEMA3A-Fc or NBQX/CPP (Figure 8) were analyzed in fixed cochleae, so it was impossible for us to determine if the increased branch numbers resulted from elevated branch sprouting or diminished branch retraction. In future studies, it will be important to incorporate time-lapse studies to examine the dynamics of SGN branch refinement under different conditions. In addition, it will be important to determine if SGNs from *Sema3a*^{K108N} mice or models where SGN activity is clearly diminished or enhanced, show changes in branch refinement.

While we found that exposing SGNs to SEMA3A *in vitro* led to effects suggestive of a role in activity modulation, the *Sema3a*^{K108N} and heterozygous control cochleae did not show significant differences in terms of Ca^{2+} transients (Figure 10). One possibility is that the imaging technique we used had limitations that prevented us from detecting subtle differences between the two genotypes. In particular, Fluo4-AM-loaded SGNs can show high levels of photobleaching and can show uneven dye loading. In addition, since we performed recordings from SGN cell bodies, we may have missed any small-scale changes that may only be detectable only around the hair cell synapse where SEMA3A is located (Figures 2 and 3). Additionally, since the activity modulation in neurons is a complex process that requires multiple internal and external cues, it is possible there were no detectable changes in activity in the *Sema3a*^{K108N} cochleae because of compensation by other Semaphorins. We previously characterized SEMA3F and SEMA5B in the context of type I SGN guidance and branch refinement.[5,10] Whether these or other Semaphorins play a role in activity modulation in the developing cochlea is an open question. Overall, as SGNs exhibit synchronized spontaneous activity during development,[35] the regulation of this activity by Semaphorins in vivo remains an exciting and important question.

Interestingly, *Sema3a*^{K108N} cochleae did not show changes in type I SGN differentiation, a process known to be dependent on activity.[11–13] But, it is possible that the role of SEMA3A in modulating SGN activity occurs at a timepoint outside of the normal period of SGN specification. Whether *Sema3a*^{K108N} mice show altered hearing acuity by auditory brainstem response (ABR) threshold is also an open question. Whereas the mutants around 1 month postnatal showed observable changes in GLUA2 patch distribution based on volume, they lacked any changes in type I SGN differentiation and showed no evidence of SGN loss (Figure 4). In addition, there were no apparent changes in hair cell Ca^{2+} influx properties (Figure 6). So, it is unlikely that the *Sema3a*^{K108N} mice would show a substantial rise in ABR thresholds. But, it is possible that subtle “suprathreshold” changes (eg, wave 1 amplitude and latency) could result from the changes in synapse distribution. Future studies will need to be carried out to address these important issues.

The results presented here on SEMA3A and type I SGNs support a model whereby different Semaphorins show differing patterns of expression and serve distinct functions in cochlear development. The downstream mechanisms that might facilitate SEMA3A-mediated changes in SGN synaptic morphology via activity modulation remain to be elucidated. One possibility is that SEMA3A modulates cell surface AMPA receptor levels, as has been shown for SEMA3F.[49] Another possibility is that SEMA3A regulates the expression of pre- and postsynaptic machinery, as has been shown for SEMA4D in the context of hippocampal GABAergic synapses in the hippocampus.[53] Another possibility is that SEMA3A may directly modulate K^+ and Ca^{2+} currents, as was suggested by pharmacology experiments using cultured SGNs.[24] Future research will delineate these and other possibilities.

4 | EXPERIMENTAL PROCEDURES

4.1 | Mouse lines

All mice were maintained in accordance with the Institutional Animal Care and Use Committee at Georgetown University (#1147). For the morphometric analyses and cochlear culture experiments, mice carrying the *R26R*^{tdTomato} reporter allele (Jackson Laboratories, stock #007914) were crossed with mice carrying *Neurog1*^{CreERT2}.[4] *Neurog1*^{CreERT2} were a kind gift from Dr. Lisa Goodrich, Harvard University. Together these alleles yield stochastic labeling of SGNs in the absence of tamoxifen.[5,10] *Neurog1*^{CreERT2}; *R26R*^{tdTomato} mice were crossed with *Sema3a*^{K108N} mutants[25] for single SGN morphometric analyses. The *Sema3a*^{K108N} mouse line was purchased from Jackson Laboratories (stock # 014646) and maintained on a C57BL/6 N background (using Charles River strain 556). *Neurog1*^{CreERT2}; *Rosa26*^{tdTomato} were of mixed background. For the *Sema3*a *in situ* hybridization studies and Sema3A/Nrp1 protein expression studies, timed-pregnant NIH Swiss mice (Charles River Laboratories) were used. In all experiments, male and female mice were used. In Figure 1A,B, where example SGNs are shown, *Bhlhb5*^{Cre} and *R26R*^{MORF3} (Jax stock# 035403) were used.[54] We and others have shown previously that *Bhlhb5*^{Cre} drives reporter alleles in SGNs and olivocochlear efferents.[10,55]

4.2 | In vitro culture of postnatal cochleae

For cochlear culture experiments, cochleae from *Neurog1*^{CreERT2}; *Rosa26*^{tdTomato} mice were carefully isolated from the inner ear at P4. For each sample, before placing them in culture medium containing Dulbecco's Modified Eagle Medium (DMEM), 10% fetal bovine serum, 0.2% N2, and 0.001% ciprofloxacin,[5] the lateral wall and extraneous connective tissues were discarded. Each cochlea was cultured for 24 hours at 37°C under 5% CO_2 while flattened on polycarbonate membrane filters (Sterlitech PCT0213100). Then, 25 nM SEMA3A-Fc chimera protein (R&D Systems 1250-S3–025), control human IgG-Fc (Jackson ImmunoResearch, 009–000-008), 5 μM AMPA receptor inhibitor NBQX (Abcam AB120160), or 10 μM NMDA receptor inhibitor CPP (Abcam 120 046) were then added to the culture medium. Following the 24 hour culture period, the cochleae were fixed in 4% paraformaldehyde (PFA) for 15 minutes then processed for immunohistochemistry and confocal microscopy.

4.3 | In situ hybridization

Cochleae from mice were carefully isolated and fixed in chilled 4% PFA overnight then rinsed in 1X PBS. Samples were treated with 10%, 20%, and 30% sucrose before being embedded in OCT Compound (Tissue-Tek). The tissue was then frozen into blocks and sectioned at 12 μm. *Sema3a* antisense and sense control probes were generated from *pYx-Asc-Sema3a* using T3 and T7 polymerase, respectively. The procedures for carrying out the probe hybridization and detection were identical to what was described previously.[56]

4.4 | Immunostaining

Cochleae were carefully removed and fixed with 4% PFA for 45 minutes then rinsed in 1X PBS. Samples were then prepared for sectioning as described in the in situ hybridization section. For whole mount immunostaining prior to P8, the cochlear capsule and lateral wall were removed. Cochleae were then permeabilized using 0.5% Triton X-100 in 1X PBS followed by 1 hour in 10% normal donkey serum at RT for blocking. Immunostaining was performed as previously described.[5] For cochleae after P8, fixation was performed by perfusing the bony capsule with 4% PFA followed by a 45-minute incubation in 4% PFA followed by rinses in 1X PBS. Cochleae were then placed in 0.125 M EDTA for 24 to 48 hours to decalcify. Antibodies used in this study include the following: mouse-anti-Tuj1 (Covance, MMS-435P; 1:500), rabbit-anti-dsRed (Clontech, 632 496; 1:2000), rabbit-anti-MyosinVI (MyoVI; Proteus Biosciences, 25–6791; 1:1000), rabbit-anti-GAP43 (Millipore, AB5220; 1:1000), goat-anti-MyoVI (1:1000,[5]), chicken-anti-neurofilament (Aves Labs, NF200, NFH; 1:2000), mouse-GLUA2 (1:500, MAB397), goat-anti-RIBEYE (Santa Cruz, sc-5967, 1:500), mouse-SEMA3A (Santa Cruz, Sc-74 554, 1:500), goat-NRP1(R&D systems, AF566, 1:250), sheep-Lypd1 (R&D Systems, AF6855, 1:500), chicken-CALB1(Abeomics, 34–1020, 1:200) and rabbit-CALB2 (ThermoFisher, PA5–34688, 1:500).

4.5 | Imaging and quantifications

Following immunohistochemistry, confocal z-stack images were taken using a Zeiss LSM-880 confocal. Micrographs of in situ hybridization samples were taken using a Nikon E800 compound scope and Nikon DXM1200 digital camera. Imaris (Bitplane) software was used to quantify SGN morphology from mice carrying *Neurog1*^{CreERT2} and *Rosa26*^{tdTomato}. For the type I SGN 3D reconstruction data found in Figures 1, 4, and 8, confocal z-stack images of SGNs were traced and reconstructed using the filaments feature in Imaris. The parameters used to identify modiolar vs pillar neurons is illustrated in Figure 1C. Primary, secondary, and tertiary branches were individually reconstructed for the data in Figure 8; the histogram indicates total branch numbers. We note here that all tdTomato-labeled protrusions coming off the main SGN fiber were considered a “branch.” Since these were static images, we were unable to distinguish structures with different biological roles (eg, branches vs filopodia) or examine their growth dynamics. Only SGNs that synapse either on the pillar or modiolar pole of the IHCs were included in this study; SGNs that synapsed on the most habenular pole of the IHCs were excluded to avoid ambiguity. Additionally, as shown in Figure 1A, SGNs typically display a varicosity before synapsing on the IHCs; analyses of thickness were done from the end of each varicosity to 50 μm down the SGNs.

Imaris was also used to analyze postsynaptic GLUA2 puncta in *Sema3a*^{K108N} mice: puncta from the modiolar or pillar cell side of each IHCs were individually reconstructed using the volume tool feature in Imaris.

4.6 | Ca^{2+} imaging

For Ca^{2+} imaging of SGN cell bodies, cochleae were dissected from postnatal day 4 WT mice in ice-cold sterile ACSF buffer (130 mM NaCl, 2.5 mM KCl, 10 mM HEPES, 1 mM NAH_2PO_4, 1.3 mM MgC_{l2}, 1.5 mM $CaCl_2$ and 11 mM D-glucose). Cochlear explants were placed (with SGNs down) on polycarbonate membrane filters (Sterlitech, Kent, Washington) and incubated at 37°C for 2 to 4 hours in DMEM buffer supplemented with 1% FBS and Ciprofloxacin hydrochloride (Sigma). Cochleae were then incubated for 2 hours in ACSF containing Flou4-AM, then rinsed with ACSF media before imaging. The preparations were then transferred to the LSM880 in ACSF media where images were captured at 1 frame per second and at 512 × 512 pixels. For the experiments shown in Figure 9, baseline recordings of cochlear activity were captured for 5 to 10 minutes before adding either SEMA3A-Fc or Control-Fc to the bath. Preparations were allowed to rest for 5 to 10 minutes before subsequent acquisitions. Analysis of Ca^{2+} transients was performed using ImageJ and MATLAB as shown previously.[36]

4.7 | Patch clamp and live imaging

Sema3a^{K108N} and WT littermate mice were used for patch clamp and live imaging experiments at age P24–30. Animal handling and experiments complied with national animal care guidelines and were approved by the University of Göttingen Board for Animal Welfare and the Animal Welfare Office of the state of Lower Saxony. IHCs from freshly dissected organ of Corti (2/3 of apical turn) were patched-clamped from either pillar or modiolar side. Patch pipettes were made from borosilicate glass (Science products, GB150F-8P) and pulled using a P-97 Flaming/Brown micropipette puller (Sutter Instruments). The pipette solution contained (in mM): 111 Cs-glutamate, 1 $MgCl_2$, 1 $CaCl_2$, 10 EGTA, 13 TEA-Cl, 20 HEPES, 4 Mg-ATP, 0.3 Na-GTP and 1 L-glutathione, pH 7.3, 290 mOsm. Additionally, Ca^{2+} indicator Fluo-4FF (0.8 mM; Life Technologies) and TAMRA-conjugated CtBP2/RIBEYE binding peptide (10 mM) were added to the intracellular solution for live imaging. Extracellular solution contained (in mM): 2.8 KCl, 105 NaCl, 10 HEPES, 1 $CsCl_2$, 1 $MgCl_2$, 5 $CaCl_2$, 35 TEA-Cl, and 2 mg/mL D-glucose, pH 7.2, 300 mOsm.

For the acquisition EPC-10 amplifier controlled by PatchMaster software (HEKA Elektronik) was used. IHCs were held at −87 mV holding potential. Voltage ramp depolarizations ranging from 87 to 63 mV within 150 ms (1 mV/ms) were applied to trigger Ca^{2+} influx. All voltages were corrected for liquid junction potential (17 mV) and voltage drops across series resistance (R_s). Recordings, which displayed leak currents above −50 pA at −87 mV, R_s above 14 MΩ during the first 3 minutes after rupturing the cell or Ca^{2+} current rundown more than 25%, were discarded from the analysis. Recordings were leak corrected using P/n protocol. All experiments were performed at room temperature (22°C-23°C).

Ca^{2+} imaging was performed with a spinning disk confocal scanner (CSU22, Yokogawa) mounted on an upright microscope (Axio Examiner, Zeiss) with ×63, 1.0 NA objective (W Plan-Apochromat, Zeiss), as previously described.[30] Images were acquired using a scientific CMOS camera with 103 × 103 nm pixel size (Neo, Andor). The spinning disk was set to 2000 rpm to synchronize with the 10 ms exposure time of the camera during Ca^{2+} imaging.

A fast piezoelectric system for objective (Piezosystem) was used to acquire z-stacks. First, the whole IHC was scanned from the basal end to the top of the cell by exciting TAMRA with 591 nm diode pumped solid state excitation laser (Cobolt AB). Laser exposure time for TAMRA imaging was 0.5 seconds and the step size for z-scanning was 0.5 μm. For Ca^{2+} imaging, the sections from the basal-most end of the cell to the plane containing the uppermost ribbon were imaged with the step size of 0.5 μm while exciting Fluo-4FF with 491 nm diode pumped solid state excitation laser (Cobolt AB). Ca^{2+} hotspots at each plane were evoked by voltage ramp depolarizations and simultaneously imaged at 100 Hz frame rate. For each plane, two different voltage ramps were applied, one being 5 ms shifted relative to the other one.

4.8 | Data analysis

4.8.1 | Patch-clamp and imaging—Data were analyzed with Igor pro 6.3 software (Wavemetrics) using custom written programs. For the analysis of IV curves the evoked Ca^{2+} current of each depolarization step was averaged over the 5 to 10 ms interval after the start of depolarization and plotted against voltage. Fractional activation curves of the whole cell Ca^{2+} currents were calculated from IV curves and fitted with Boltzmann function.

For the Ca^{2+} imaging data, 10 frames preceding the voltage ramp stimulus were averaged to make a reference image for the resting state (F_0). The image at maximal stimulation was calculated by averaging six frames between 40 and 90 ms of stimulation (F_{max}). F_0 was subtracted from F_{max} to obtain the ΔF image which allowed us to visualize the Ca^{2+} hotspots of each recorded plane. The intensity of the central pixel of the hotspot was averaged with the eight surrounding pixels at all time points to obtain the intensity profile over time. Two intensity profiles corresponding to the shifted voltage ramp stimuli were concatenated and plotted against voltage (FV curve). As the FV curves were noisy, they were refined by fitting the modified Boltzmann function:

$$F = F_0 + \frac{G_{max}(V_{rev} - V_m)}{1 + \exp\left[\frac{V_m - V_h}{k}\right]}$$

where F is the fluorescence intensity at a given voltage, F_0 is the fluorescence at a resting state, and V_m is the command voltage, V_{rev} is the reversal potential calculated from the IV recordings of whole cell patch-clamp data, V_h is the voltage of half-maximal Ca^{2+} influx, and k is the slope. The decay in the fluorescence corresponding to depolarized voltages resulted from the driving force, despite the full activation of the Ca^{2+} channels. In order to calculate the fractional activation curves, a line was fitted in the range of 3 mV to the reversal potential for each FV fit. The resulting line (G_{max} line) was extrapolated to the rest of the voltages to obtain the fluorescence intensities of maximal activation condition.

Finally, FV fit was divided by the G_{max} line and the resulted points were fitted with Boltzmann function:

$$F = \frac{1}{1 + \exp\left[\frac{V_m - V_h}{k}\right]}$$

To measure fluorescence intensity of the synaptic ribbon (visualized by TAMRA-conjugated dimeric Ctbp2 binding peptide), the highest fluorescence pixel intensity was divided by the intensity of the ribbon's nearby pixel (F_{ribbon}/F_{nearby}).

The suction force of the pipette deforms the cell shape while patching and induces variability in morphologies, thus making it difficult to pool the data from different cells together. To overcome that difficulty, images were transferred from the canonical Cartesian coordinate system into a self-defined polar coordinate system.[30] Briefly, symmetry vector of the cell (V_{sym}), which also replaces tonotopic axis in this case, was calculated. Next, the cell was sectioned along the plane of symmetry and a vector parallel to the pillar edge of the cell was assigned (V_{pillar}). The cell was resectioned along V_{pillar} and the centers of mass of the bottom-most plane and the largest plane were connected to define the central vector (V_z). The cross product of V_{sym} and V_z produced the vector defining pillar-modiolar axis (V_{pm}). Finally, the coordinates of ribbons were calculated in polar coordinate system and plotted in polar charts. The two orthogonal axes of polar charts show pillar-modiolar and apical-basal (referring to the tonotopic axis) axes of the cell.

ACKNOWLEDGMENTS

The authors wish to thank members of the Coate, Vicini and Moser laboratories for helpful comments on the manuscript. The authors also thank Dr Elisabeth Glowatzki and lab members (Johns Hopkins University, Baltimore, MD) for their insight and helpful suggestions throughout this project.

FUNDING INFORMATION

This work was supported by NIH R00 DC13107 (T. M. C.), and NIH R01 DC016595 (T. M. C.), the Mathers Foundation (T. M. C.), and funding from the Georgetown School of Arts and Sciences (H. L. C.). Deutsche Forschungsgemeinschaft (DFG, German Research Foundation) under Germany's Excellence Strategy—EXC 2067/1-390729940 as well as by the Leibniz Program of the DFG (T. M.).

Funding information

Deutsche Forschungsgemeinschaft (DFG, German Research Foundation) under Germany's Excellence Strategy, Grant/Award Number: EXC 2067/1-390729940; G. Harold and Leila Y. Mathers Charitable Foundation, Grant/Award Number: MF-1804-00065; National Institute on Deafness and Other Communication Disorders, Grant/Award Numbers: DC016595, DC13107

REFERENCES

1. Arnesen AR, Osen KK. The cochlear nerve in the cat: topography, cochleotopy, and fiber spectrum. J Comp Neurol. 1978; 178(4):661–678. doi:10.1002/cne.901780405 [PubMed: 632375]
2. Liberman MC. Single-neuron labeling in the cat auditory nerve. Science. 1982;216(4551):1239–1241. doi:10.1126/science.7079757 [PubMed: 7079757]
3. Kelly M, Chen P. Shaping the mammalian auditory sensory organ by the planar cell polarity pathway. Int J Dev Biol. 2007; 51(6–7):535–547. doi:10.1387/ijdb.072344mk [PubMed: 17891715]

4. Koundakjian EJ, Appler JL, Goodrich LV. Auditory neurons make stereotyped wiring decisions before maturation of their targets. J Neurosci. 2007;27(51):14078–14088. doi:10.1523/JNEUROSCI.3765-07.2007 [PubMed: 18094247]

5. Coate TM, Spita NA, Zhang KD, Isgrig KT, Kelley MW. Neuropilin-2/semaphorin-3F-mediated repulsion promotes inner hair cell innervation by spiral ganglion neurons. Elife. 2015;4 (AUGUST2015):1–24. doi:10.7554/eLife.07830

6. Liberman MC. Central projections of auditory-nerve fibers of differing spontaneous rate. I. Anteroventral cochlear nucleus. J Comp Neurol. 1991;313(2):240–258. doi:10.1002/cne.903130205 [PubMed: 1722487]

7. Liberman MC. Auditory-nerve response from cats raised in a low-noise chamber. J Acoust Soc Am. 1978;63(2):442–455. doi: 10.1121/1.381736 [PubMed: 670542]

8. Simmons DD, Liberman MC. Afferent innervation of outer hair cells in adult cats: I. light microscopic analysis of fibers labeled with horseradish peroxidase. J Comp Neurol. 1988;270(1):132–144. doi:10.1002/cne.902700111 [PubMed: 3372735]

9. Weisz CJC, Lehar M, Hiel H, Glowatzki E, Fuchs PA. Synaptic transfer from outer hair cells to type II afferent fibers in the rat cochlea. J Neurosci. 2012;32(28):9528–9536. doi:10.1523/JNEUROSCI.6194-11.2012 [PubMed: 22787038]

10. Jung JS, Zhang KD, Wang Z, et al. Semaphorin-5b controls spiral ganglion neuron branch refinement during development. J Neurosci. 2019;39(33):6425–6438. doi:10.1523/JNEUROSCI.0113-19.2019 [PubMed: 31209173]

11. Sun S, Babola T, Pregernig G, et al. Hair cell mechanotransduction regulates spontaneous activity and spiral ganglion subtype specification in the auditory system. Cell. 2018;174(5):1247–1263.e15. doi:10.1016/j.cell.2018.07.008 [PubMed: 30078710]

12. Shrestha BR, Chia C, Wu L, Kujawa SG, Liberman MC, Goodrich LV. Sensory neuron diversity in the inner ear is shaped by activity. Cell. 2018;174(5):1229–1246.e17. doi:10.1016/j.cell.2018.07.007 [PubMed: 30078709]

13. Petitpré C, Wu H, Sharma A, et al. Neuronal heterogeneity and stereotyped connectivity in the auditory afferent system. Nat Commun. 2018;9(1):3691. doi:10.1038/s41467-018-06033-3 [PubMed: 30209249]

14. Luo Y, Raible D, Raper JA. Collapsin: a protein in brain that induces the collapse and paralysis of neuronal growth cones. Cell. 1993;75(2):217–227. doi:10.1016/0092-8674(93)80064-L [PubMed: 8402908]

15. Gu C, Rodriguez ER, Reimert DV, et al. Neuropilin-1 conveys semaphorin and VEGF signaling during neural and cardiovascular development. Dev Cell. 2003;5(1):45–57. doi:10.1016/S1534-5807(03)00169-2 [PubMed: 12852851]

16. He Z, Tessier-Lavigne M. Neuropilin is a receptor for the axonal chemorepellent semaphorin III. Cell. 1997;90(4):739–751. doi:10.1016/S0092-8674(00)80534-6 [PubMed: 9288753]

17. Kolodkin AL, Levengood DV, Rowe EG, Tai YT, Giger RJ, Ginty DD. Neuropilin is a semaphorin III receptor. Cell. 1997; 90(4):753–762. doi:10.1016/S0092-8674(00)80535-8 [PubMed: 9288754]

18. Soker S, Takashima S, Miao HQ, Neufeld G, Klagsbrun M. Neuropilin-1 is expressed by endothelial and tumor cells as an isoform-specific receptor for vascular endothelial growth factor. Cell. 1998;92(6):735–745. doi:10.1016/S0092-8674(00)81402-6 [PubMed: 9529250]

19. Gu C, Limberg BJ, Brian Whitaker G, et al. Characterization of neuropilin-1 structural features that confer binding to semaphorin 3A and vascular endothelial growth factor 165. J Biol Chem. 2002;277(20):18069–18076. doi:10.1074/jbc.M201681200 [PubMed: 11886873]

20. Salehi P, Ge MX, Gundimeda U, et al. Role of neuropilin-1/semaphorin-3A signaling in the functional and morphological integrity of the cochlea. PLoS Genet. 2017;13:e1007048. doi: 10.1371/journal.pgen.1007048, 10.1371/journal.pgen.1007048

21. Yamashita N, Usui H, Nakamura F, et al. Plexin-A4-dependent retrograde semaphorin 3A signalling regulates the dendritic localization of GluA2-containing AMPA receptors. Nat Commun. 2014;5:1–7. doi:10.1038/ncomms4424

22. Sasaki Y, Cheng C, Uchida Y, et al. Fyn and Cdk5 mediate semaphorin-3A signaling, which is involved in regulation of dendrite orientation in cerebral cortex. Neuron. 2002;35(5):907–920. doi:10.1016/S0896-6273(02)00857-7 [PubMed: 12372285]

23. Taniguchi M, Nagao H, Takahashi YK, et al. Distorted odor maps in the olfactory bulb of semaphorin 3A-deficient mice. J Neurosci. 2003;23(4):1390–1397. doi:10.1523/jneurosci.23-04-01390.2003 [PubMed: 12598627]
24. Wong VSC, Meadows M, Goldberg D, Willis DE. Semaphorin 3A induces acute changes in membrane excitability in spiral ganglion neurons in vitro. Eur J Neurosci. 2019;50(1):1741–1758. doi:10.1111/ejn.14360 [PubMed: 30706560]
25. Merte J, Wang Q, Vander Kooi CW, et al. A forward genetic screen in mice identifies Sema3AK108N, which binds to neuropilin-1 but cannot signal. J Neurosci. 2010;30(16):5767–5775. doi:10.1523/JNEUROSCI.5061-09.2010 [PubMed: 20410128]
26. Meyer AC, Frank T, Khimich D, et al. Tuning of synapse number, structure and function in the cochlea. Nat Neurosci. 2009; 12(4):444–453. doi:10.1038/nn.2293 [PubMed: 19270686]
27. Liberman LD, Liberman MC. Postnatal maturation of auditory-nerve heterogeneity, as seen in spatial gradients of synapse morphology in the inner hair cell area. Hear Res. 2016;339:12–22. doi:10.1016/j.heares.2016.06.002 [PubMed: 27288592]
28. Katayama K-I, Imai F, Suto F, Yoshida Y. Deletion of Sema3a or plexinA1/plexinA3 causes defects in sensory afferent projections of statoacoustic ganglion neurons. PLoS One. 2013;8(8):1–6. doi:10.1371/journal.pone.0072512
29. Sherrill HE, Jean P, Driver EC, et al. Pou4f1 defines a subgroup of type i spiral ganglion neurons and is necessary for normal inner hair cell presynaptic Ca2+ signaling. J Neurosci. 2019; 39(27):5284–5298. doi:10.1523/JNEUROSCI.2728-18.2019 [PubMed: 31085606]
30. Ohn TL, Rutherford MA, Jing Z, et al. Hair cells use active zones with different voltage dependence of Ca2+ influx to decompose sounds into complementary neural codes. Proc Natl Acad Sci U S A. 2016;113(32):E4716–E4725. doi:10.1073/pnas.1605737113 [PubMed: 27462107]
31. Zenisek D, Horst NK, Merrifield C, Sterling P, Matthews G. Visualizing synaptic ribbons in the living cell. J Neurosci. 2004; 24(44):9752–9759. doi:10.1523/JNEUROSCI.2886-04.2004 [PubMed: 15525760]
32. Wong AB, Rutherford MA, Gabrielaitis M, et al. Developmental refinement of hair cell synapses tightens the coupling of Ca2+ influx to exocytosis. EMBO J. 2014;33(3):247–264. doi:10.1002/embj.201387110 [PubMed: 24442635]
33. Koppel AM, Feiner L, Kobayashi H, Raper JA. A 70 amino acid region within the semaphorin domain activates specific cellular response of semaphorin family members. Neuron. 1997;19(3):531–537. doi:10.1016/S0896-6273(00)80369-4 [PubMed: 9331346]
34. Babola TA, Li S, Gribizis A, et al. Homeostatic control of spontaneous activity in the developing auditory system. Neuron. 2018;99(3):511–524.e5. doi:10.1016/j.neuron.2018.07.004 [PubMed: 30077356]
35. Zhang-Hooks YX, Agarwal A, Mishina M, Bergles DE. NMDA receptors enhance spontaneous activity and promote neuronal survival in the developing cochlea. Neuron. 2016;89(2):337–350. doi:10.1016/j.neuron.2015.12.016 [PubMed: 26774161]
36. Caccavano A, Lorenzo Bozzelli P, Forcelli PA, et al. Inhibitory parvalbumin basket cell activity is selectively reduced during hippocampal sharp wave ripples in a mouse model of familial Alzheimer's disease. J Neurosci. 2020;40(26):5116–5136. doi:10.1523/JNEUROSCI.0425-20.2020 [PubMed: 32439703]
37. Appler JM, Lu CC, Druckenbrod NR, Yu WM, Koundakjian EJ, Goodrich LV. Gata3 is a critical regulator of cochlear wiring. J Neurosci. 2013;33(8):3679–3691. doi:10.1523/JNEUROSCI.4703-12.2013 [PubMed: 23426694]
38. Coate TM, Raft S, Zhao X, Ryan AK, Crenshaw EB, Kelley MW. Otic mesenchyme cells regulate spiral ganglion axon fasciculation through a Pou3f4/EphA4 signaling pathway. Neuron. 2012;73(1):49–63. doi:10.1016/j.neuron.2011.10.029 [PubMed: 22243746]
39. Druckenbrod NR, Hale EB, Olukoya OO, Shatzer WE, Goodrich LV. Neuronal processes and glial precursors form a scaffold for wiring the developing mouse cochlea. Nat Commun. 2020;11(1):1–11. doi:10.1038/s41467-020-19521-2 [PubMed: 31911652]

40. Defourny J, Poirrier AL, Lallemend F, et al. Ephrin-A5/EphA4 signalling controls specific afferent targeting to cochlear hair cells. Nat Commun. 2013;4:1438. doi:10.1038/ncomms2445 [PubMed: 23385583]
41. Mao X, Ou MT, Karuppagounder SS, et al. Pathological α-synuclein transmission initiated by binding lymphocyte-activation gene 3. Science. 2016;353(6307):aah3374. doi:10.1126/science.aah3374
42. Wang Z, Jung JS, Inbar TC, Rangoussis KM, Faaborg-Andersen C, Coate TM. The purinergic receptor p2rx3 is required for spiral ganglion neuron branch refinement during development. eNeuro. 2020;7(4):1–21. doi:10.1523/ENEURO.0179-20.2020
43. Kim KX, Rutherford MA. Maturation of nav and kv channel topographies in the auditory nerve spike initiator before and after developmental onset of hearing function. J Neurosci. 2016; 36(7):2111–2118. doi:10.1523/JNEUROSCI.3437-15.2016 [PubMed: 26888923]
44. Sendin G, Bulankina AV, Riedel D, Moser T. Maturation of ribbon synapses in hair cells is driven by thyroid hormone. J Neurosci. 2007;27(12):3163–3173. doi:10.1523/JNEUROSCI.3974-06.2007 [PubMed: 17376978]
45. Yang C, Tang D. Patient-specific carotid plaque progression simulation. Comput Model Eng Sci. 2000;1(2):119–131. doi:10.1016/j.biotechadv.2011.08.021.Secreted
46. Erskine L, François U, Denti L, et al. VEGF-A and neuropilin 1 (NRP1) shape axon projections in the developing CNS via dual roles in neurons and blood vessels. Development. 2017; 144(13):2504–2516. doi:10.1242/dev.151621 [PubMed: 28676569]
47. Low LK, Liu XB, Faulkner RL, Coble J, Cheng HJ. Plexin signaling selectively regulates the stereotyped pruning of corticospinal axons from visual cortex. Proc Natl Acad Sci U S A. 2008;105(23):8136–8141. doi:10.1073/pnas.0803849105 [PubMed: 18523013]
48. Bagri A, Cheng HJ, Yaron A, Pleasure SJ, Tessier-Lavigne M. Stereotyped pruning of long hippocampal axon branches triggered by retraction inducers of the semaphorin family. Cell. 2003;113(3):285–299. doi:10.1016/S0092-8674(03)00267-8 [PubMed: 12732138]
49. Wang Q, Chiu SL, Koropouli E, et al. Neuropilin-2/PlexinA3 receptors associate with GluA1 and mediate Sema3F-dependent homeostatic scaling in cortical neurons. Neuron. 2017;96(5):1084–1098.e7. doi:10.1016/j.neuron.2017.10.029 [PubMed: 29154130]
50. Torborg CL, Feller MB. Spontaneous patterned retinal activity and the refinement of retinal projections. Prog Neurobiol. 2005; 76(4):213–235. doi:10.1016/j.pneurobio.2005.09.002 [PubMed: 16280194]
51. Faust T, Gunner G, Schafer DP. Mechanisms governing activity-dependent synaptic pruning in the developing mammalian CNS. Nat Rev Neurosci. 2022;22(11):657–673. doi:10.1038/s41583-021-00507-y.Mechanisms
52. Simon D, O'Leary D. Limited topographic specificity in the targeting and branching of mammalian retinal axons. Dev Biol. 1990;137(1):125–134. doi:10.1016/0012-1606(90)90013-9 [PubMed: 1688537]
53. Serrano Cardona L, Muñoz ME. Paraninfo Digital. Early Hum Dev. 2013;83(1):1–11. doi:10.1016/j.earlhumdev.2006.05.022
54. Veldman MB, Park CS, Eyermann CM, et al. Brainwide genetic sparse cell labeling to illuminate the morphology of neurons and glia with Cre-dependent MORF mice. Neuron. 2020;108(1): 111–127.e6. doi:10.1016/j.neuron.2020.07.019 [PubMed: 32795398]
55. Ross SE, Mardinly AR, McCord AE, et al. Loss of inhibitory interneurons in the dorsal spinal cord and elevated itch in Bhlhb5 mutant mice. Neuron. 2010;65(6):886–898. doi:10.1016/j.neuron.2010.02.025 [PubMed: 20346763]
56. Driver EC, Pryor SP, Hill P, et al. Hedgehog signaling regulates sensory cell formation and auditory function in mice and humans. J Neurosci. 2008;28(29):7350–7358. doi:10.1523/JNEUROSCI.0312-08.2008 [PubMed: 18632939]

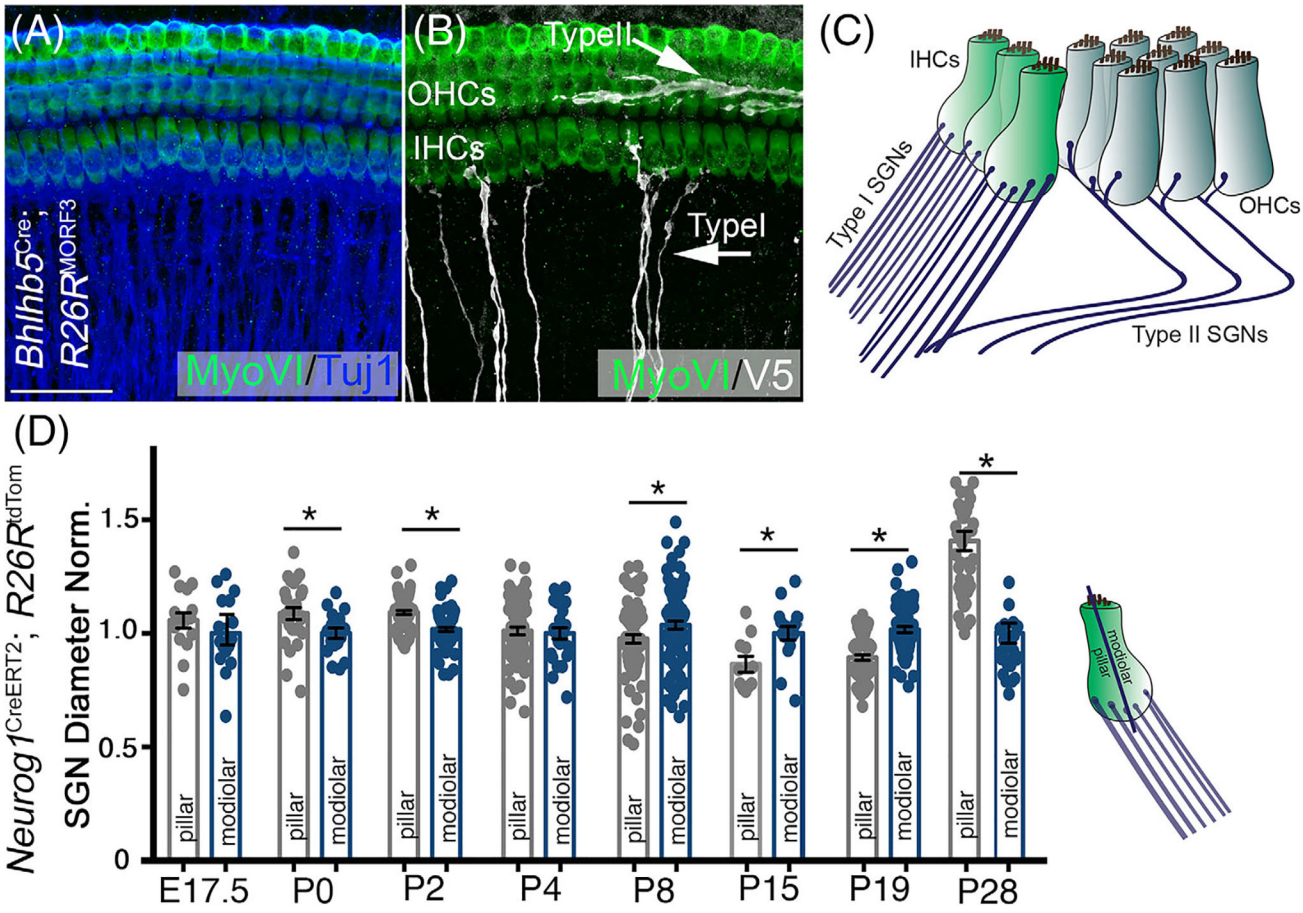

FIGURE 1.

Type I spiral ganglion neurons (SGNs) vary in thickness over the course of development. (A) A whole-mount view of SGNs and hair cells shown by Tuj1 and MyoVI staining, respectively, from a mouse carrying *Bhlhb5*^{Cre}; *R26R*^{MORF3}. (B) The same sample with SGN sparse labeling from anti-V5 immunostaining. Note the variation in fiber thickness. (C) Schematic of the organ of Corti, showing one row of inner hair cells (IHCs) and three rows of OHCs which are innervated by type I SGNs and type II SGNs, respectively. (D) Developmental analysis of type I SGNs that make contact on either the modiolar or pillar side of the inner hair cell using whole-mounts from sparsely-labeled *Neurog1*^{CreERT2}; *R26R*^{tdtomato} cochleae starting at E17.5 through P28. Values shown on the histograms were normalized to the average diameter of the SGN fibers synapsing on the modiolar side of the IHC. (Student's *t* test; mean ± SEM; *$P \leq .05$, **$P \leq .01$, ***$P \leq .001$.) Each dot represents one fiber; for statistical tests, we used the average from each cochlea as one biological replicate. For each stage, 3 to 15 cochleae were used. Scale bar (in (A)): approx. 40 μm

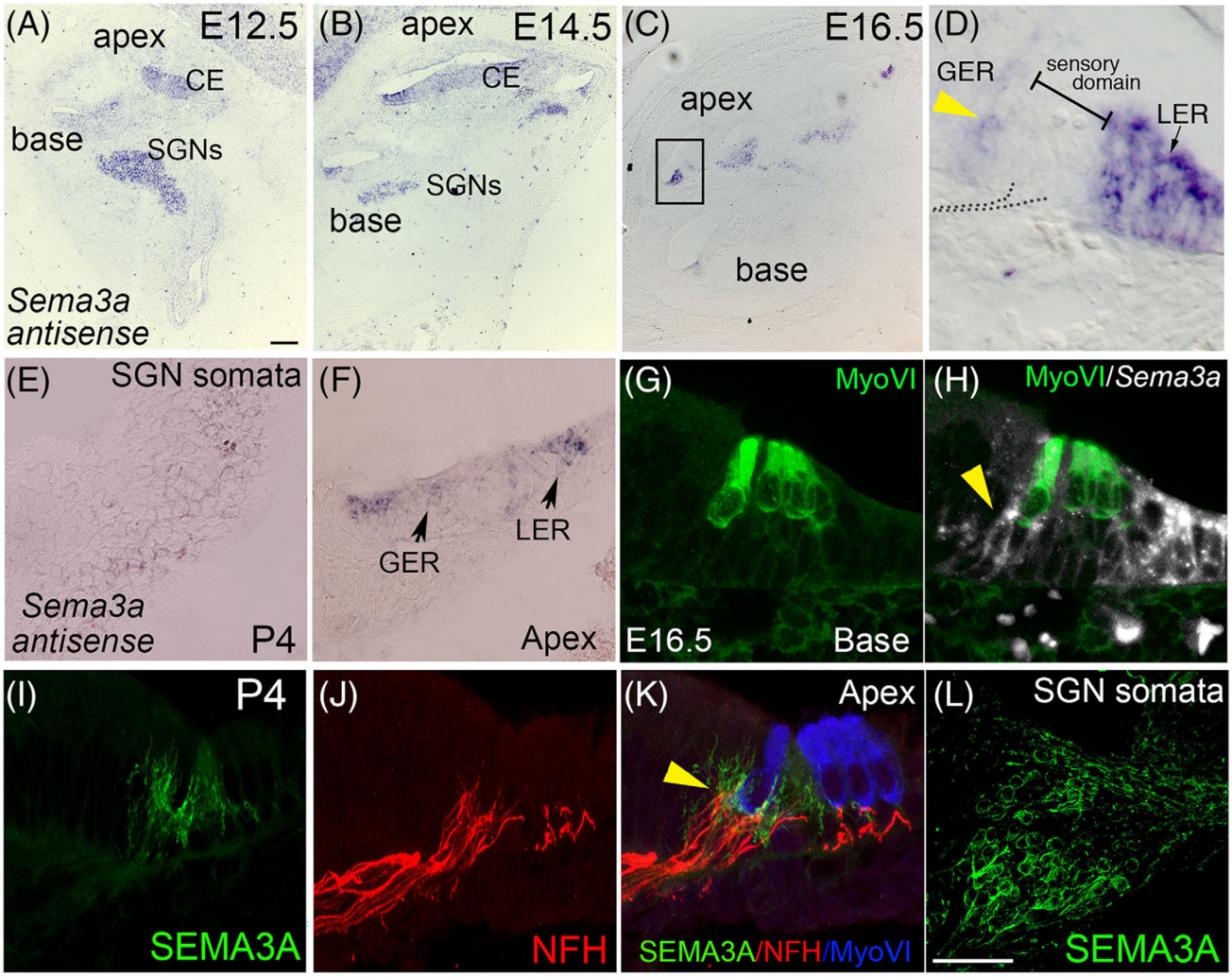

FIGURE 2.

Sema3a/Semaphorin-3A (SEMA3A) developmental expression in the cochlea. (A-F) In situ hybridization showing *Sema3a* expression in the cochlea across different developmental days. (A, B) At E12.5 and E14.5, *Sema3a* transcripts are visible in spiral ganglion neuron (SGN) cell bodies and around the developing sensory domain. (C, D) *Sema3a* transcripts are visible in cells surrounding the hair cells, specifically in the lesser epithelial ridge (LER) and greater epithelial ridge (GER) regions. Panel (D) is a high-magnification view from the boxed region in (C), but flipped horizontally to match the orientation of other panels in this figure. Dotted lines represent location of SGNs. *Sema3a* transcripts are detectable (but at lower levels compared to other stages) in the SGN cell bodies (E) and cochlear epithelial cells (F) at P4. (G) Anti-MyoVI immunostaining of an E16.5 cochlear cross section shows the position of the hair cells. (H) Overlap of *Sema3a* mRNA anti-MyoVI antibody staining shows that *Sema3a* is expressed in regions surrounding the hair cells. (I-L) SEMA3A immunostaining of P4 cochlear cross sections. (I) Anti-SEMA3A antibody labeling appears in a filament-like manner that overlaps with NFH staining, but not MyoVI staining (J, K). (L) SGN cell bodies at P4 show SEMA3A immunoreactivity. Scale bar in (A) (applies to A-C), approx. 120 μm. Scale bar in (L) (applies to D-L): 30 μm in (D), 60 μm in (E) and (F),

30 μm in (G-K), 60 μm in (L) (all approx.). The yellow arrowheads point to inner phalangeal cells expressing *Sema3a* mRNA in (D) and (H), and SEMA3A protein in (K)

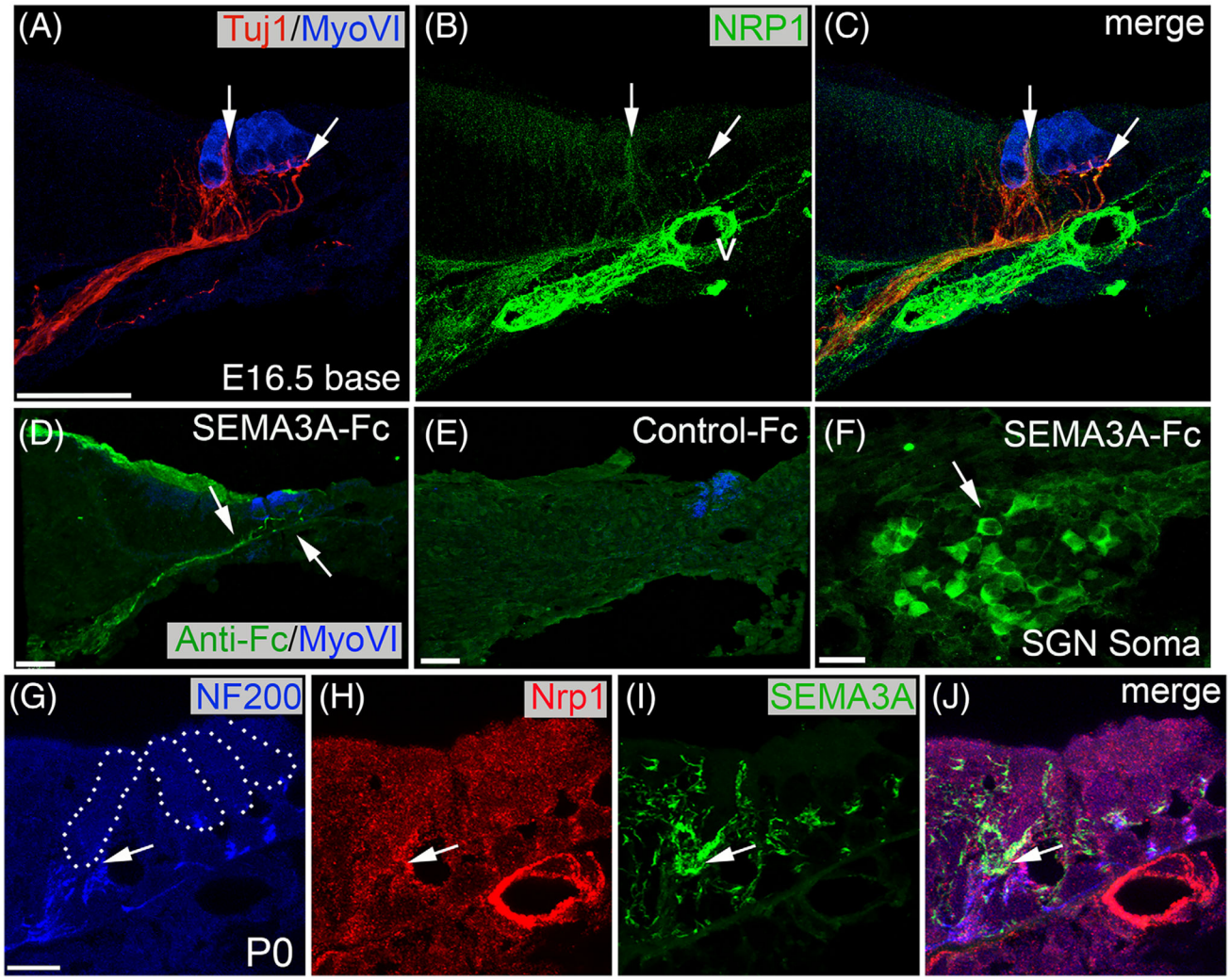

FIGURE 3.

Semaphorin-3A (SEMA3A)-Fc binds to NRP1 expressing spiral ganglion neurons (SGNs). (A-C) NRP1, a known SEMA3A receptor, is expressed by SGNs and blood vessels. (A) Cochlear cross section at E16.5 labeled with Tuj1 and MyoVI antibodies to show the distribution of SGNs and hair cells, respectively. (B) Anti-NRP1staining is visible on SGN fibers (arrows) and blood vessels (V). (C) Merged view of (A) and (B). (D) Lightly fixed E17.5 cochlear cross section treated with SEMA3A-Fc, the processed for anti-Fc immunostaining. The white arrows point at anti-Fc-positive SGNs. (E) Similar to (D), but with Control-Fc showing no staining. (F) Anti-Fc-labeled SGN cell bodies of cochlear cross sections treated with SEMA3A-Fc. (G-J) Cochlear cross section at P0 labeled with (G) anti-NF200, (H) anti-NRP1 and (I) anti-SEMA3A. The white arrows point at the synaptic area of the inner hair cells (IHCs) where all three proteins are visible. Scale bar (in A, D, and E): approx. 20 μm. (F) approx. 25 μm. (G) approx. 10 μm

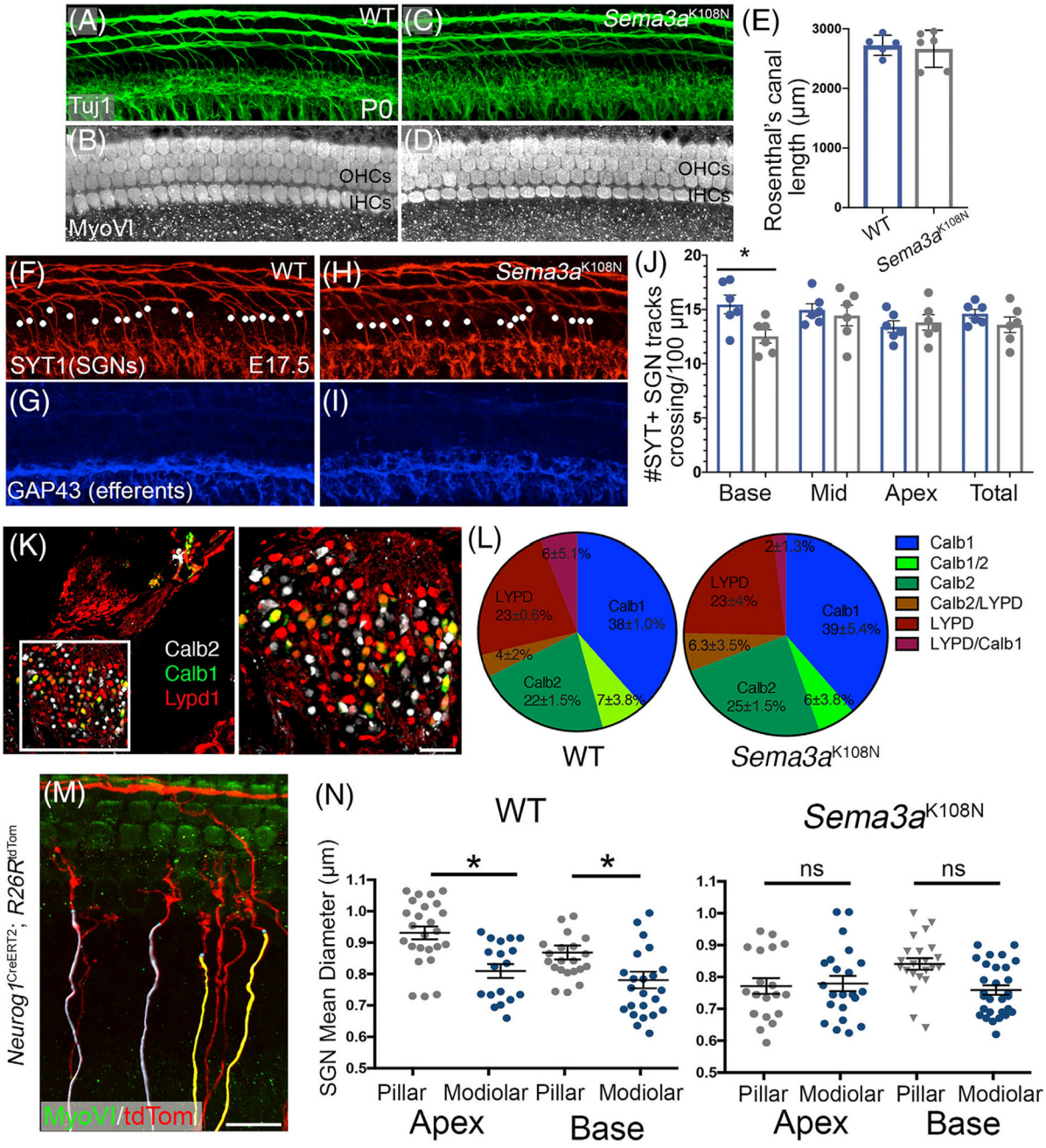

FIGURE 4.

Sema3a^{K108N} mice show an abnormal distribution of type I spiral ganglion neurons (SGNs) based on their fiber diameter. (A-D) P0 whole-mount views of cochleae from WT (A, B) and *Sema3a*^{K108N} (C, D) mice stained with anti-MyoVI to label hair cells and anti-Tuj1 to label SGNs. Overall patterns of innervation and hair cell formation are normal. (E) Histogram showing no difference in the length of Rosenthal's canal between WT and *Sema3a*^{K108N} cochleae (Student's *t* test; mean ± SEM; $^{**}P \leq .01$; n = 5 WT and 6 *Sema3a*^{K108N} cochleae). (F, G) A WT cochlea at E17.5 shows the normal distribution of SYT1-positive SGNs, and GAP43-positive olivocochlear efferents around the hair cell region. (H, I) Overall,

Sema3a^{K108N} cochleae appear similar to controls with these markers. The white dots indicate fibers crossing into the outer hair cell region. (J) Histogram showing the number of SYT1 positive fibers crossing into the outer hair cell region is slightly reduced only in the base of the cochlea (Student's *t* test; mean ± SEM; ***P* ≤ .01; n = 5 WT cochleae; 6 *Sema3a*^{K108N} cochleae). (K, L) *Sema3a*^{K108N} cochleae show no altered type I SGN subtype marker distribution. (K) Representative image of P30 WT cochleae cross section with Calb2, Calb1, and LYPD1 cell body labeling to show three different Type I SGN subtypes. (L) Pie chart showing proportions in WT and *Sema3a*^{K108N} cochlea positive for one or two of subtype markers. Student's *t* test; mean ± SEM; **P* ≤ .05, ***P* ≤ .01, ****P* ≤ .001; control samples; n = 6; *Sema3a*^{K108N} samples; n = 7). Scale bar in (A), approx. 30 μm. (M) Example of Imaris fiber diameter reconstruction of a P2 *Neurog1*^{CreERT2}; *R26R*^{tdtomato} cochleae labeled with MyoVI and dsRed antibodies. (N) Type I SGN fiber diameters based on synaptic position for WT and *Sema3a*^{K108N} cochleae (Student's *t* test; mean ± SEM; ***P* ≤ .01; n = 8 WT cochlea; 8 *Sema3a*^{K108N} cochlea). Scale bar in (M): approx. 40 μm for (A-D) and (F-I); 25 μm in (K). In *Sema3a*^{K108N} cochleae, the normal spatial distribution of SGNs based on their fiber diameter was absent. ns = not significant

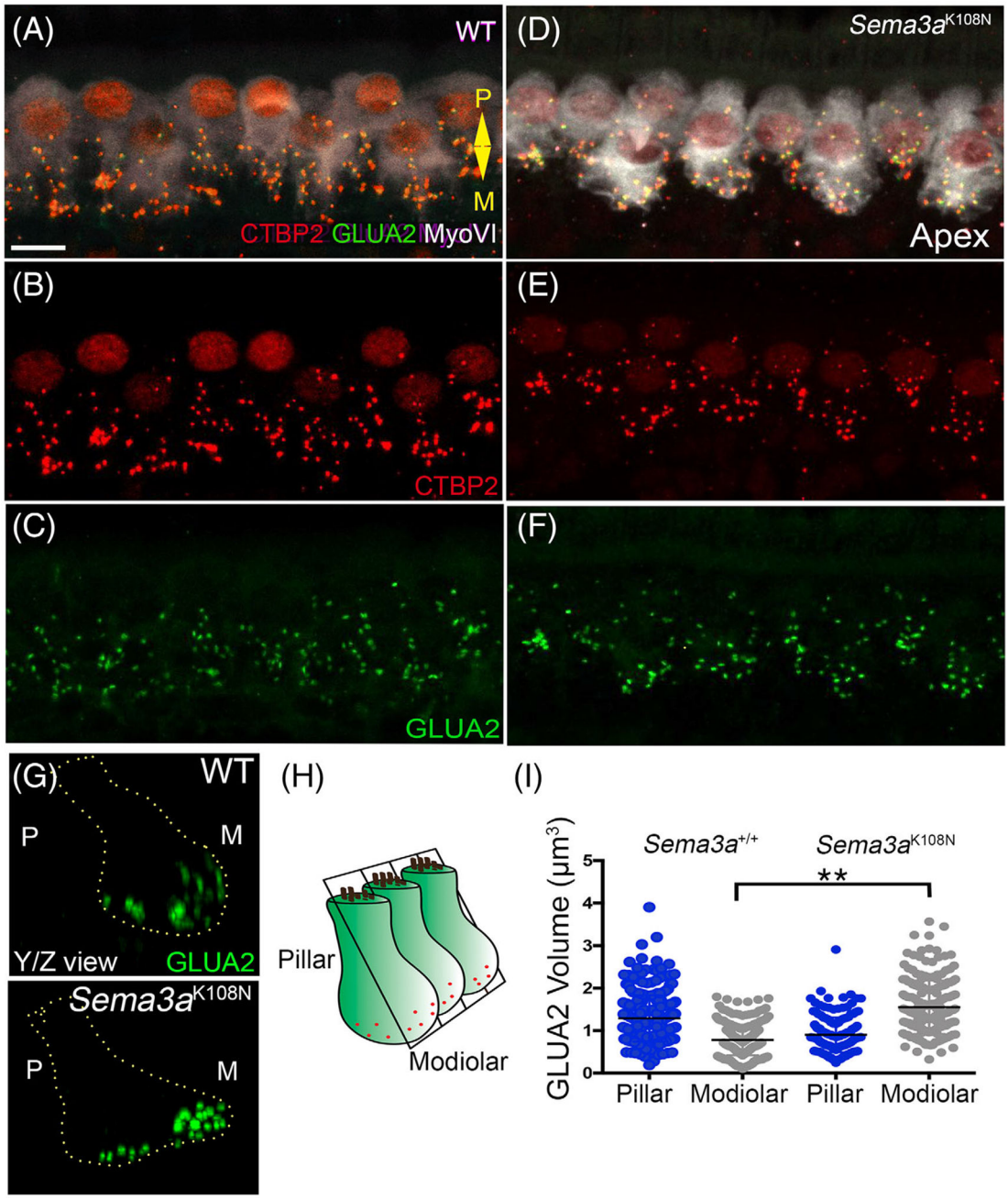

FIGURE 5.

Sema3a^{K108N} mice show larger volume GLUA2 patches on the modiolar side of the inner hair cell (IHC). (A-F) P30 whole mount cochleae from WT (A-C) and *Sema3a*^{K108N} mice (D-F) stained with anti-MyoVI to label hair cells, anti-CTBP2 for presynaptic ribbons, and GLUA2 for postsynaptic contacts. (G) WT and *Sema3a*^{K108N} orthogonal view (from the confocal z-stack) of example inner hair cells labeled with anti-GLUA2. The dotted yellow lines follow the contours of the IHC. (H) Schematic depicting the division criteria of "modiolar" and "pillar" IHC sides. (I) Histogram showing the distribution of GLUA2 puncta by volume on each side of the IHC for each genotype. Each dot represents the average

synapse volume for one IHC. Contrary to controls, the largest GLUA2 puncta were found on the modiolar side of IHC in *Sema3a*^{K108N} cochleae (Student's *t* test; mean ± SEM; $^{**}P \leq .01$; n = 8 WT cochlea; 9 *Sema3a*^{K108N} cochlea). Scale bar (in A): approx. 40 μm

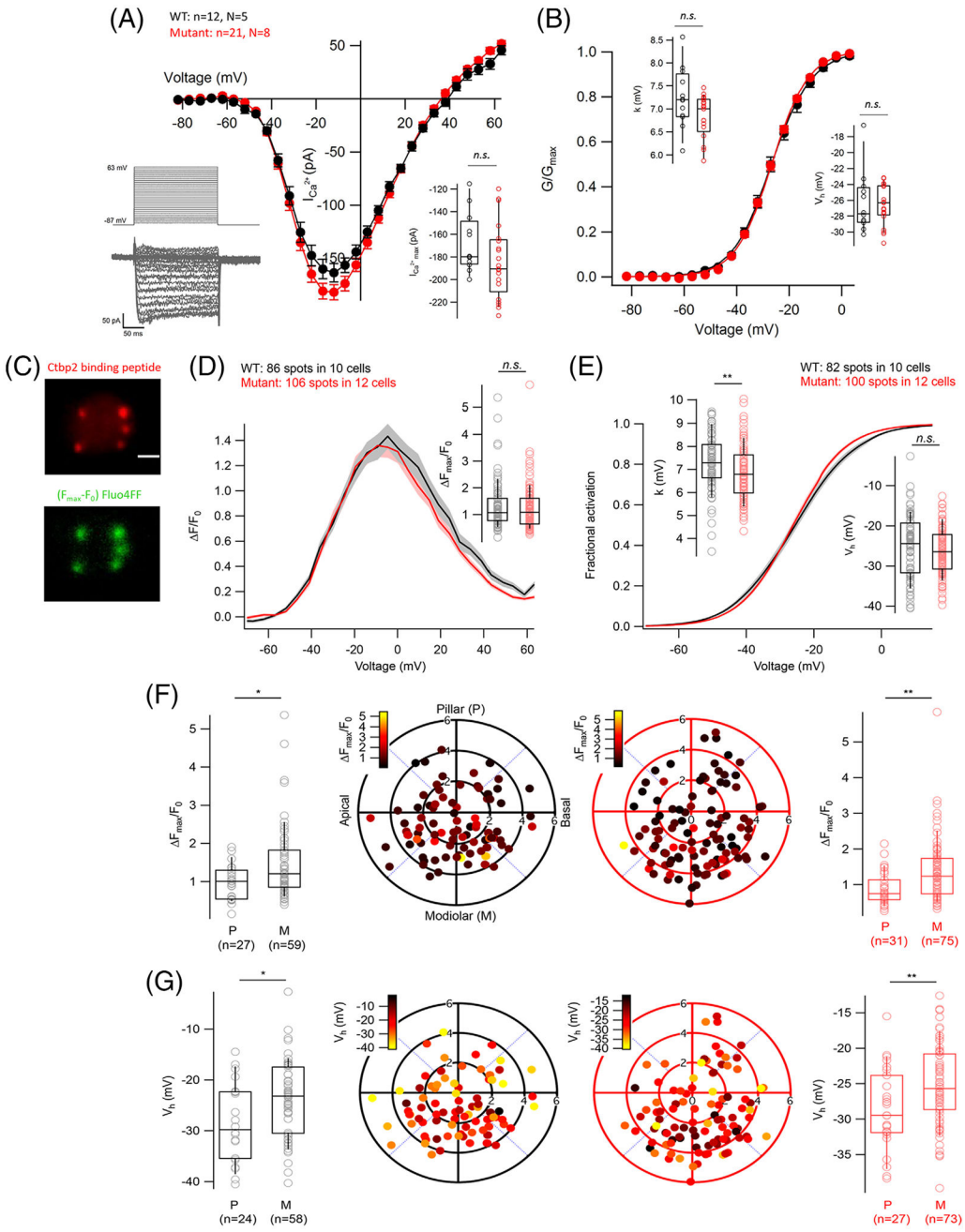

FIGURE 6.

Inner hair cells (IHCs) of *Sema3a*^{K108N} and WT show comparable whole cell Ca^{2+} currents. (A) IV relationships showing normal Ca^{2+} currents in IHCs of *Sema3a*^{K108N} mice (mean ± SEM). Protocol of step-depolarizations and resulting whole cell currents (bottom left). Box-whisker plots showing no difference in the maximum amplitude of Ca^{2+} currents between IHCs of WT and *Sema3a*^{K108N} mice (bottom right) ($P = .11$, Mann-Whitney-Wilcoxon test). (B) Fractional activation curves calculated from IV relationship and fitted with Boltzmann function show no difference between IHCs of WT and *Sema3a*^{K108N} mice. Box-whisker plots show no change in the voltage sensitivity (k; $P = .09$, Mann-Whitney-

Wilcoxon test) or voltage of half maximal activation (V_h; $P = .57$, Mann-Whitney-Wilcoxon test) in IHCs of *Sema3a*^{K108N} mice. Box-whisker plots with individual IHC data points overlaid show median (middle line), 25 and 75th percentiles (lower and upper borders of the box) and 10th and 90th percentiles (whiskers). Spatial gradients of maximum Ca^{2+} influx and V_h remain intact in IHCs of *Sema3a*^{K108N} mice. (C) Single IHC plane showing fluorescence of TAMRA conjugated CtBP2/RIBEYE binding peptide (upper image) and corresponding Ca^{2+} hotspots evoked by voltage ramp protocols (lower image). Scale bar = 2 μm. (D) Average $\Delta F/F_0$ traces at individual synapses plotted against depolarization voltages (FV relationship) show no difference between single synaptic Ca^{2+} influx in WT and *Sema3a*^{K108N} IHCs. Shaded areas represent ±SEM. Box-whisker plots show no difference in maximum amplitude of Ca^{2+} influx ($\Delta F_{max}/F_0$) at individual synapses in WT and Sema3a^{K108N} IHCs, calculated by averaging five values at the FV peak ($P = .59$, Mann-Whitney-Wilcoxon test). (E) Fractional activation curves calculated from the fits of FV relationship. Shaded areas represent ±SEM. Box-whisker plots show increased voltage sensitivity (k; $P = .006$, Mann-Whitney-Wilcoxon test) and no change in voltage of half maximal activation (V_h; $P = .33$, Mann-Whitney-Wilcoxon test) at individual active zones of *Sema3a*^{K108N} IHCs. (F) Polar charts showing positions of individual synapses in WT (left, black) or mutant (right, red) IHCs. Pseudo-color scale displays maximum fluorescence of Ca^{2+} influx. Box-whisker plots displaying $\Delta F_{max}/F_0$ distributions of pillar and modiolar synapses show stronger Ca^{2+} influx at modiolar synapses compared to pillar synapses in both WT ($P = .025$, Mann-Whitney-Wilcoxon test) and *Sema3a*^{K108N} IHCs ($P = .001$, Mann-Whitney-Wilcoxon test). (G) Polar charts showing positions of individual synapses in WT (left, black) or mutant (right, red) IHCs. Pseudo-color scale displays V_h. Box-whisker plots displaying V_h distributions of pillar and modiolar synapses show more depolarized Ca^{2+} influx at modiolar synapses compared to pillar synapses in both WT ($P = .014$, Mann-Whitney-Wilcoxon test) and *Sema3a*^{K108N} IHCs ($P = .008$, Mann-Whitney-Wilcoxon test). Box-whisker plots with individual active zone data points overlaid show median (middle line), 25th and 75th percentiles (lower and upper borders of the box) and 10th and 90th percentiles (whiskers)

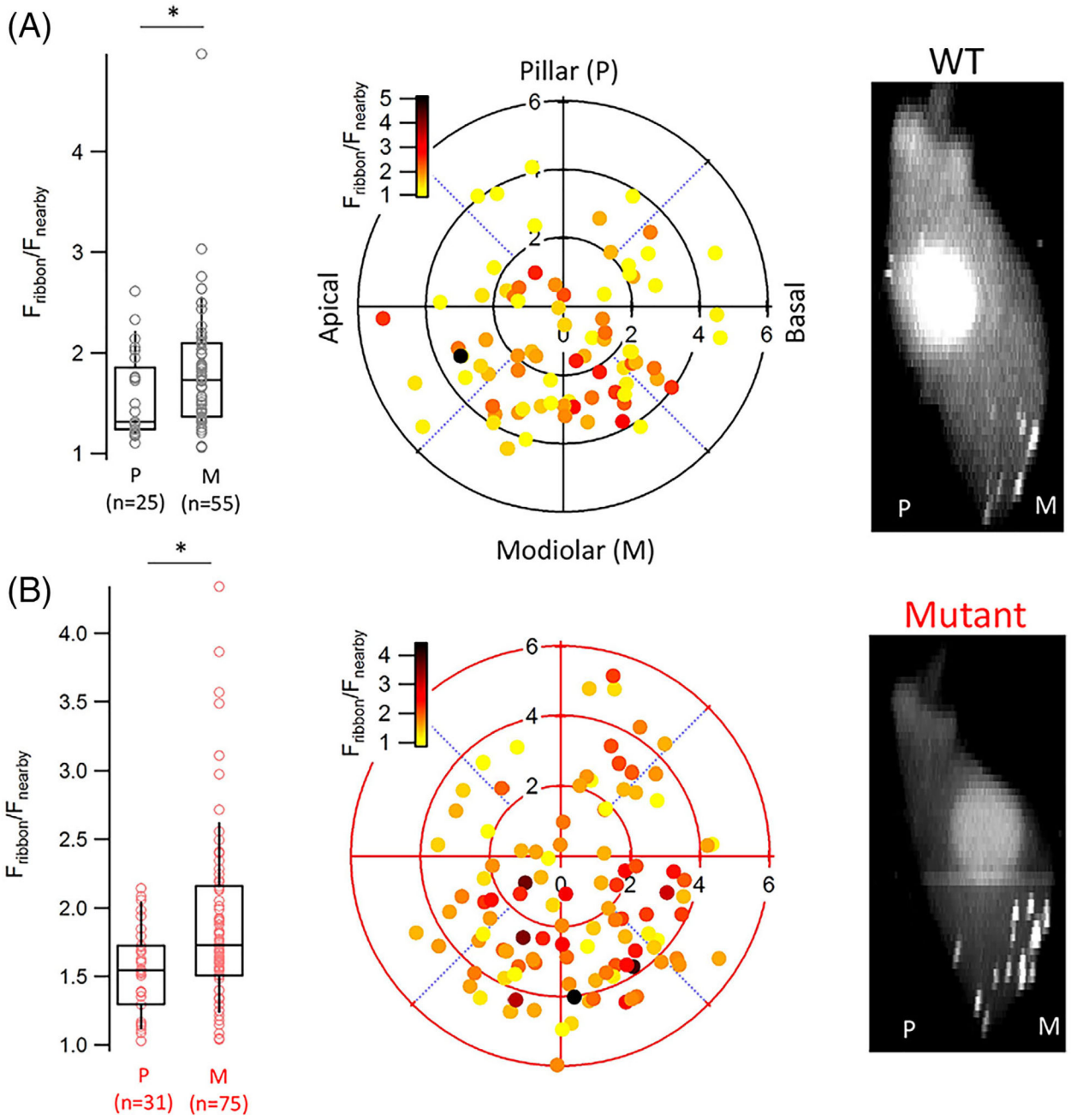

FIGURE 7.

Spatial gradient of ribbon size in inner hair cells (IHCs) of *Sema3a*^{K108N} mice obtained with live imaging. (A, B) Box-whisker plots displaying ribbon size distributions of pillar and modiolar synapses show bigger ribbons at the modiolar side of the IHC compared to pillar the pillar side in WT (A) and *Sema3a*^{K108N} (B) mice. Polar charts showing positions of individual synapses in WT (A) and *Sema3a*^{K108N} (B) IHCs. Pseudo-color scale displays highest fluorescence pixel intensity of the ribbon normalized to the intensity of the ribbon's nearby pixel. Maximum intensity projection of the IHCs along their symmetry vector, filled up with TAMRA-conjugated CtBP2/RIBEYE binding peptide

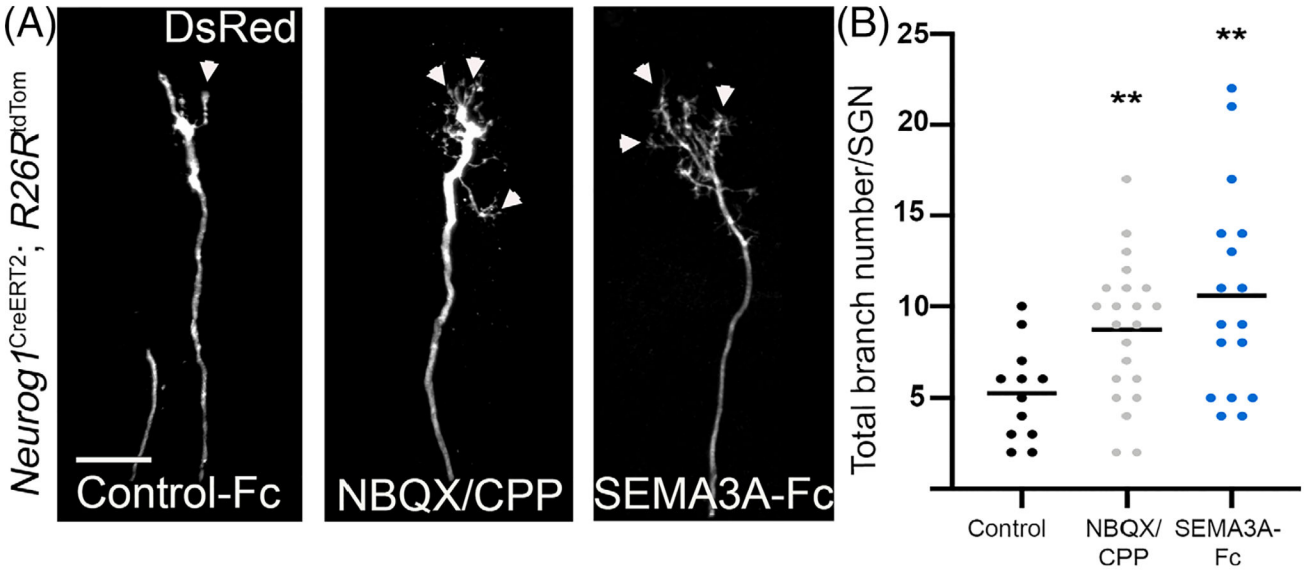

FIGURE 8.

Spiral ganglion neurons (SGNs) from cultured cochleae show extra branches after exposure to Semaphorin-3A (SEMA3A) and NBQX/CPP. (A) Sample images of cochleae from *Neurog1*^{CreERT2}, *R26R*^{tdTomato} mice cultured at P4 and exposed to Control-Fc (20 nM), SEMA3A-Fc (20 nM), or NBQX/CPP (5 μM/10 μM). (B) SGNs cultured with SEMA3A-Fc and NBQX/CPP show significantly higher branch numbers compared to controls. (Student's *t* test; mean ± SEM; $*P \leq .05$, $**P \leq .01$, $***P \leq .001$.) For the histograms, each dot represents one fiber analyzed; statistics were performed using the average for each cochlea; eight cochleae were used per condition. Scale bar in (A), 10 μm

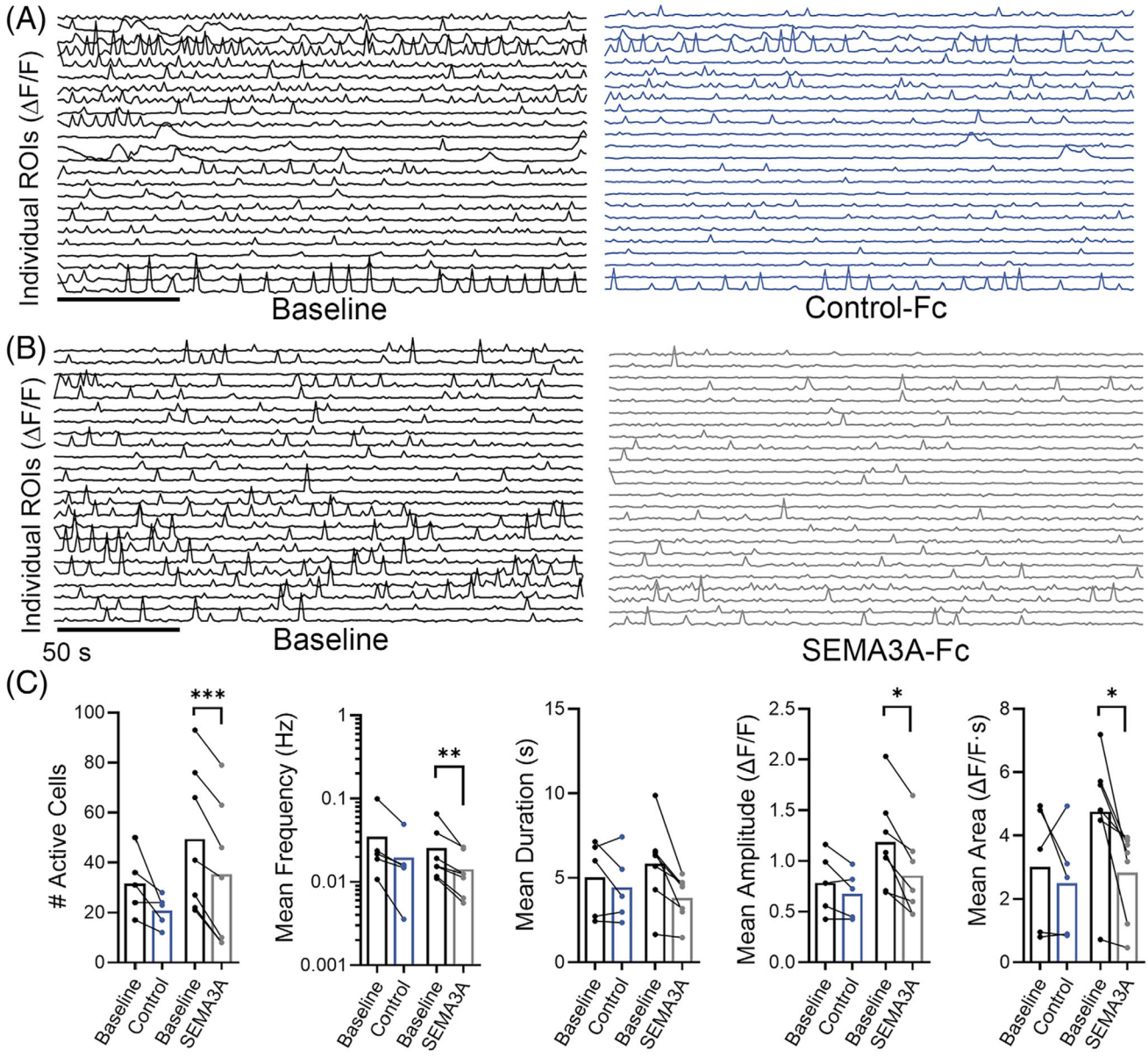

FIGURE 9.

Cultured P4 cochleae show reduced Ca^{2+} activity after exposure to Semaphorin-3A (SEMA3A)-Fc. (A, B) Sample MATLAB traces from Fluo4-AM-treated cochleae showing individual ROIs before and after exposure to Control-Fc (A) and SEMA3A-Fc (B). (C) Summary plot of number of active cells. SEMA3A-Fc reduces the number of active cells (two-way analysis of variance with Bonferroni correction; mean ± SEM; $*P \leq .05$, $**P \leq .01$, $***P \leq .001$; control samples; n = 11; SEMA3A-Fc samples; n = 10). For statistics, each biological replicate (n = 1) represents the average values of ROIs for each cochlea. Subsequent analysis of frequency, amplitude and duration were computed only using active cells. *Mean frequency*. SEMA3A-Fc exposed cochlea showed a significant decrease on frequency compared to its own baseline values. *Mean duration*. Average fluorescence duration is not significantly reduced in cochleae exposed to SEMA3A-Fc when compared

to its own baseline values. *Mean amplitude*. Average fluorescence amplitude is significantly reduced on cochleae exposed to SEMA3A-Fc when compared to its own baseline values. Control-Fc exposed cochleae show no significant difference compared to baseline levels despite the mild bleaching. *Mean area*. Average area is significantly reduced in cochlea exposed to SEMA3A-Fc when compared to its own baseline values

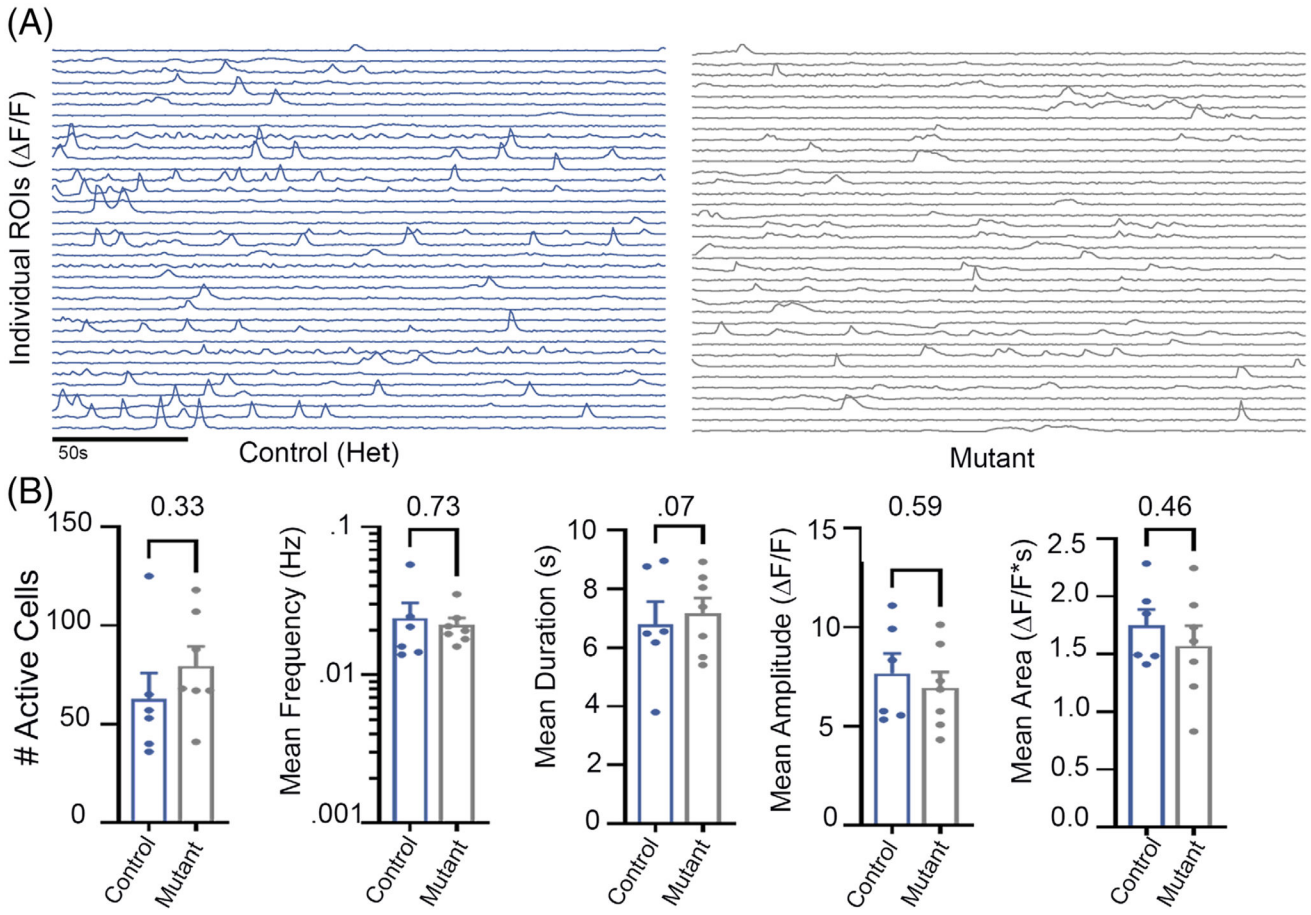

FIGURE 10.

Sema3a^{K108N} cochleae show no significant changes in spiral ganglion neuron (SGN) Ca^{+2} transients. (A) Sample MATLAB traces from Fluo4-AM-treated cochleae showing individual ROIs of *Sema3a*^{K108N} mutants and heterozygous littermates used as controls. (B) Summary plots. There were no significant changes on the number of active cells, mean frequency, mean duration, mean amplitude, or mean area between control heterozygous and *Sema3a*^{K108N} (Student's *t* test; mean ± SEM; $*P \leq .05$, $**P \leq .01$, $***P \leq .001$; control samples; n = 7; *Sema3a*^{K108N} samples; n = 6). For statistics, each biological replicate (n = 1) represents that average values of ROIs for each cochlea